# A new look to the old solvent: Mass transfer performance and mechanism of $CO_2$ absorption into pure monoethanolamine in a spray column

Emine Kayahan[1], Ulderico Di Caprio[1], Annelot Van den Bogaert[1], Mohammed N. Khan[2], Metin Bulut[2], Leen Braeken[1], Tom Van Gerven[3], M. Enis Leblebici[1,*]

[1] *Center for Industrial Process Technology, Department of Chemical Engineering, KU Leuven, Agoralaan Building B, 3590 Diepenbeek, Belgium*

[2] *Business Unit Separation and Conversion Technology, Flemish Institute for Technological Research (VITO), Boeretang 200, 2400 Mol, Belgium*

[3] *Process Engineering for Sustainable Systems, Department of Chemical Engineering, KU Leuven, Celestijnenlaan 200F, B-3001 Heverlee, Belgium*

*Corresponding author (muminenis.leblebici@kuleuven.be)

## Abstract

The most mature $CO_2$ capture technology is absorption of monoethanolamine (MEA) in packed or spray columns. Typically, an aqueous 30 wt.% MEA solution is used. High MEA concentrations are believed to hinder mass transfer rate due to high viscosity of MEA. We worked, for the first time, on the effects of using pure MEA on overall mass transfer coefficient ($K_G a$) and absorption efficiency in a spray column by varying several operational parameters. Image analysis results suggested that interfacial area increased with increasing liquid flow rate. As a result, $K_G a$ increased. As opposed the belief in literature, $K_G a$ also increased with increasing MEA concentrations. The highest $K_G a$ was obtained in this work (11.7 $kmol \cdot m^{-3} \cdot kPa^{-1} \cdot h^{-1}$) is around one order of magnitude higher than most other literature studies. Having more MEA molecules on the surface of the droplets led to higher $K_G a$. In addition, it was shown that absorption efficiency was largely determined by inlet $CO_2$ to MEA molar ratio. $^{13}$C-NMR spectra results revealed that similar levels of carbamate was formed for MEA concentrations up to 70 wt.%. A simplified analysis on regeneration heat duty showed that decreasing water amount can lead to 3-10 fold decrease in reboiler energy duty.

**Keywords:** $CO_2$ capture, ethanolamine, ultrasonic nozzle, mass transfer, absorption efficiency

## 1. Introduction

As a response to the consequences of greenhouse gases on climate change, a rapid approach is sought to limit the release of $CO_2$ from flue gases into the atmosphere. There are three major approaches for carbon capture: pre-combustion capture, post-combustion capture and oxyfuel processes. Post-combustion capture has the advantage of utilizing existing combustion technologies with relatively minor changes. Among the post-combustion technologies, chemical absorption is the most well-established one that has already been implemented in oil, gas and chemical industries for the removal of $CO_2$ and $H_2S$ [1,2]. Among the various reactive solvents used for chemical absorption of $CO_2$, aqueous amine solutions are considerably well-developed [2]. However, high regeneration costs of aqueous amine solutions prevent its widespread application for $CO_2$ removal [3,4].

An aqueous 30 wt.% monoethanolamine (MEA) solution is considered as a benchmark in $CO_2$ absorption studies [1,5–9]. The absorption of $CO_2$ into MEA is a fast reaction. As a result, mass transfer limits the process performance. Overall mass transfer coefficient ($K_G a$) is often used as a performance indicator since it determines the column height. Thus, it is related to capture cost. Conventionally, the process is studied in packed bed columns. Due to the high viscosity and corrosivity of MEA, high MEA concentrations were avoided in packed columns [2,9,10]. Afkhamipour and Mofarahi [2] reviewed the mass transfer performance in terms of $K_G a$ for $CO_2$ absorption by amine solutions in packed columns. Many researchers reported that increasing liquid flow rates and MEA concentrations increased $K_G a$. Increasing liquid flow rate is usually associated with increase in the interfacial area since the wetted area on the packing increases. Both increasing liquid flow rate and concentration of chemical absorbent lead to more available absorbent molecules for $CO_2$ absorption, which, in turn, increase $K_G a$ [11–17]. Gas flow rate did not affect $K_G a$ much [13–17]. As $CO_2$ partial pressure in the flue gas increased, $K_G a$ decreased [11–17]. These results indicate that the liquid phase resistance controls the mass transfer performance of $CO_2$ absorption [2,11–17].

Spray reactors are less susceptible to corrosion due to the lack of column internals. They have less pressure drop and can be cheaper if long residence time is not required. Spray columns lack expensive

packing materials, which is expected to result in lower capital costs compared to packed columns. In addition, they can handle precipitations and can create a large interfacial area. Despite these advantages, there are only a few studies in the literature with spray columns. The reason for this might be that safety of spray reactors has not been explored much. The lower and upper explosion limits of aerosols of amines need to be known before testing industrial flue gases. Once the explosion limits are known, this issue can be tackled relatively easily. Kuntz and Aroonwilas [9] performed the first study on $CO_2$ capture in a spray reactor using MEA in 2008. They found that $K_G a$ varies significantly with gas flow rate, liquid flow rate, $CO_2$ loading, $CO_2$ partial pressure and size of the spray nozzle. In addition, the authors compared the performance of a packed column and a spray column under identical conditions. Spray reactor removed $CO_2$ at a higher rate than a packed column by a factor of 2-7. The authors worked with MEA concentrations up to 43 wt.%. An increase in $K_G a$ was observed with increasing MEA concentrations [9]. Other researchers focused on improving the mass transfer rates by changing the hydrodynamic conditions inside the spray columns. Creating a vortex flow enhanced $K_G a$ up to 33% compared to non-vortex flow in a multistage spray column when ammonia was used as an absorbent [18]. In another study, an improvement of up to 49% in $CO_2$ absorption into an aqueous NaOH solution was observed by creating swirling flows [19].

Improving $K_G a$ is one aspect of the $CO_2$ capture research. Most research is centered around finding new solvents in order to lower the regeneration energy penalty while keeping a high $CO_2$ absorption capacity and a high rate of $CO_2$ absorption [2,3,20–22]. Somewhere along the line, researchers realized that replacing water with another physical absorbent can improve $K_G a$ and decrease reboiler heat duties. Water-lean solvents, previously known as hybrid solvents, are usually a mixture of amines and organic diluents. As the name suggests, their common property is that they have less or no water content [20]. Since water-lean solvents can couple the physical and chemical absorption, early studies in this field argued that $CO_2$ absorption capacity would be higher in water-lean solvents [23,24]. However, this was not observed for low-to-moderate $CO_2$ partial pressures (up to 600 kPa) [25,26]. Most of the regular post-combustion $CO_2$ capture applications have $CO_2$ partial pressures lower than 600 kPa. Therefore, the higher absorption capacity of water-lean solvents cannot be observed in regular applications [27]. It is argued that water-lean solvents are expected to result in less reboiler heat duties because some organic diluents are less volatile and have lower heat capacities [20,25,27]. In the literature, waterless $CO_2$ capture has only been performed with

water-lean solvents. Here, we are using the term waterless capture to refer to $CO_2$ capture with both water-lean solvents and pure chemical absorbents. Below, we first discuss how to increase the absorption capacities with waterless $CO_2$ capture. Then, we elaborate on the impact of waterless $CO_2$ capture on reboiler heat duties.

In systems with both aqueous and water-lean solvent, typically, 30 wt.% of the solution absorbs $CO_2$ by chemical absorption and the rest of the solution absorbs $CO_2$ by physical absorption. Using pure chemical absorbents has the potential to boost the absorption capacities while keeping most of the advantages and eliminating some of the disadvantages brought by waterless $CO_2$ capture with water-lean solvents. Although this sounds intuitive and simple, it has not been investigated so far. Most researchers believe that the mass transfer will be hindered to prohibitively low values at high MEA concentrations due to the high viscosity of MEA. Wanderley and Knuutila [27] studied the effects of viscosity on the mass transfer rates for several water-lean solvents that rely on carbamate formation using rigorous penetration model calculations. They argued that viscosity rather than $CO_2$ solubility determines the performance of the solvent. For example, propylene glycol which has a high $CO_2$ solubility but also a high viscosity resulted in a low penetration depth and low mass transfer coefficients. They also showed that Henry's law coefficient drops significantly with increasing viscosity [27]. Although viscosity seems to decrease the mass transfer coefficients in water-lean solvents, it is not clear if increasing viscosity by using more chemical absorbent decrease mass transfer rates. Another disadvantage brought by using water-lean solvents is the shift in the vapor-liquid equilibrium curve towards less $CO_2$ absorption. This phenomenon is related to the increased destabilization of carbamate in water-lean solvents. The electrolyte stabilization in solvents is related to the combined effects of dipole-dipole interactions, van der Waals forces and hydrogen-bonding forces. [25,28]. Therefore, it is not easy to predict how using pure chemical absorbents (e.g. pure MEA) affect the mass transfer rates. In fact, because of the dilution with a physical absorbent, absorption capacity of the same amount of solvent is lowered, which leads to more solution being needed to achieve a similar $CO_2$ removal. The requirement of more solution leads to higher pumping costs, larger absorption and desorption columns and higher regeneration costs. Indeed, in a previous study performed in ASPEN plus, increasing the MEA concentration from 30 to 40 wt.% decreased the thermal energy requirements by 5-8%. In addition, with increasing MEA

concentration, cooling water and solvent consumption decreased [4]. Therefore, to what extent using pure MEA affects $K_G a$ and absorption efficiencies need to be investigated further.

Regeneration costs are the main cost item in $CO_2$ capture with amines [3,4]. De Meyer and Bignaud [29] calculated that two molecules of MEA and sixteen molecules of water need to be heated to warm up one molecule of $CO_2$ to desorb $CO_2$ from a 30 wt.% aqueous MEA solution. They assumed that all MEA molecules reacted with $CO_2$ [29]. Therefore, if the high absorption rate can be maintained without water, the heat required to warm up the water molecules will be eliminated. In addition, the heat capacity of aqueous MEA solutions decreases when the MEA wt.% increases [30]. Therefore, the regeneration costs might decrease significantly with the use of pure MEA.

As discussed above, the common practice of using diluted MEA solutions needs to be revised. Spray columns are more appropriate especially for pure chemical absorbents such as MEA since they can handle high viscosities and are less prone to corrosion. Ultrasonic nozzles are a good candidate for such applications since they can handle high viscosities and usually have a high aerosol volume concentration [31]. In addition, a wide range of stoichiometric ratios can be adjusted with the ultrasonic nozzles without compromising the quality of the nebulization since ultrasonic nozzles do not require a certain gas to liquid ratio to nebulize the liquid. In this paper, we aimed to examine the effects of $CO_2$ absorption into pure MEA on $K_G a$ and absorption efficiency. We studied several parameters such as gas flow rate, liquid flow rate, $CO_2$ concentration in the flue gas and MEA concentration with an ultrasonic nozzle. The effects of viscosity, surface tension and liquid flow rate on the droplet sizes and the interfacial areas were studied using a high-speed camera and rail system. With the droplet size analysis, the quality of the nebulization and the effect of interfacial areas on $K_G a$ were revealed. In addition, we aimed to reveal the mechanism of $CO_2$ capture into varying concentrations of MEA by $^{13}$C-NMR spectra. We presented a simplified reboiler heat duty analysis to assess the impact of using higher MEA concentrations on the economics of the overall process.

## 2. Methods

### 2.1. Viscosity and surface tension measurements

Viscosities and surface tension of aqueous MEA (Sigma Aldrich) and aqueous propylene glycol (PG, Sigma Aldrich) solutions were measured at various concentrations. Viscosity measurements were carried out with a Fungilab™ Alpha Series L Model Rotational Viscometer. The rotational viscometer offers a precision of ±1%. The viscosity of MEA solutions was recorded after 20 minutes. Surface tension was measured with Kruss DSA 10 MK2 with the pendant drop method.

### 2.2. Droplet size analysis

Droplet size analyses of aqueous PG at several concentrations and water at several liquid flow rates were done by a high-speed camera (Pyrooptic, Denmark) and a rail system (Igus, Belgium), which was controlled with a computer. A diaphragm pump (KNF, Simdos 10) was used during the analysis. The camera set-up is shown in Figure 1. One pixel was 2.47 µm. At least five pixels are needed to make a circle around the droplets. Therefore, theoretically, the camera system can detect droplets with a minimum diameter of 4.0 µm. In optical measurement methods, less droplets can be detected as the droplets approach to the lower detection limit of the camera. We checked the droplet diameters where the counting efficiency starts decreasing with another camera which can detect droplets with a diameter of 2.5 µm. The counting efficiency of the camera used in this work starts decreasing after around 11 µm. The depth of field (DOF) of the camera was found as 0.64 mm with a calibration ruler which was placed with 45$^{o}$ angle at the focal point of the camera. The field of view (FOV) of the camera was (3.2 x 2.4 mm). As a result, the camera could see a volume of 4.9 $mm^{-3}$.

Images were analyzed with Fiji which is an open source image processing package based on ImageJ2 [32]. A background image with no droplets was taken and subtracted from the images. Watershed separation was applied to separate the overlapping droplets. A macro code was written in JavaScript language and implemented to Fiji for automating the image analysis. Around five thousand images were taken at each position within five minutes of acquisition per position. The measurements of droplet sizes were done from -24 mm to +24 mm in every 3 mm inside the spray. Since the reactor diameter was 40 mm,

aerosol number concentrations (number of droplets per unit volume) from -18 mm to +18 mm were averaged. The droplet sizes were reported by combining the data from all the positions. The number and volume weighted probability density distributions for the droplet diameters were found by using MATLAB 2020b [33]. All graphs were depicted in MATLAB 2020b.

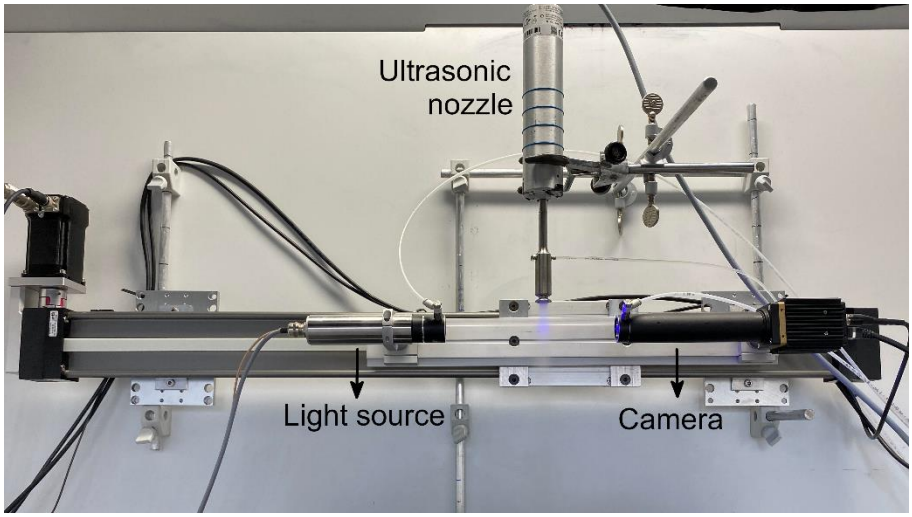


Figure 1. The high-speed camera with a pulsating LED light source and the rail system.

### 2.3. $CO_2$ capture set-up

The setup for the $CO_2$ capture experiments and the flow chart of the setup are shown in Figure 2a and b, respectively. The $CO_2$ flow rate was controlled with two mass flow controllers: Bronkhorst EL-FLOW Prestige for flow rates up to 2 $L \cdot min^{-1}$ and Bronkhorst EL-FLOW Prestige MFC for flow rates up to 80 $L \cdot min^{-1}$. The $N_2$ flow rate was controlled with Bronkhorst EL-FLOW Select MFC for flow rates up to 2 $L \cdot min^{-1}$ and Bronkhorst EL-FLOW Prestige MFC for flow rates up until 100 $L \cdot min^{-1}$. They were calibrated at a temperature of 21°C. Gas flow rates were reported in terms of normal liters. Pressure regulators were used before the mass flow controllers to adjust the pressure of the gas according to the calibration of the mass flow controllers which ranged between 1 and 3 bar gauge depending on the mass flow controller. Both gas flows were combined before entering the reactor. The gases entering the reactor were at atmospheric pressure.

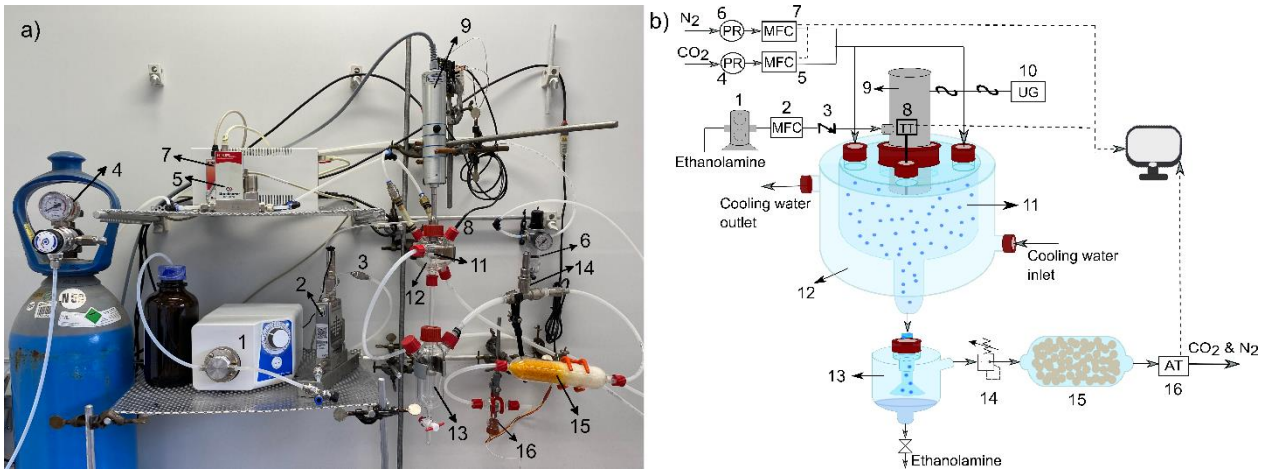


Figure 2. Experimental set-up for $CO_2$ capture in a spray reactor a) a photo of the set-up, b) process flow chart. PR, MFC, AT and UG denote pressure controller, mass flow controller, analyzer transmitter and ultrasound generator, respectively. The set-ups consists of (1) pump, (2) liquid mass flow controller, (3) check valve, (4) $CO_2$ pressure regulator, (5) $CO_2$ mass flow controller, (6) $N_2$ pressure regulator, (7) $N_2$ mass flow controller, (8) temperature sensor, (9) ultrasonic nebulizer, (10) ultrasound generator, (11) reactor, (12) cooling jacket around the reactor, (13) liquid-gas separation unit, (14) safety pressure valve, (15) silica dryer, and (16) $CO_2$ sensor.

MEA solution was pumped with a Masterflex analog gear pump system. The liquid flow rate was measured with Bronkhorst mini CORI-FLOW Coriolis mass flow controller. The liquid was nebulized with an ultrasonic nozzle, which constituted of the ultrasonic processor UP200St and the sonotrode S26d18S made of titanium (Hielscher Ultrasonics GmbH). The frequency of the ultrasonic nozzle was 26 kHz [34]. The nebulizer did not require a gas inlet. A valve was used after the pump to prevent the liquid from going back to the bottle after the process was stopped.

Both the gas mixture and the nebulized liquid were brought into contact in the glass reactor where the chemical absorption of $CO_2$ by MEA took place. The reactor had a volume of 56 ml. The length of the reactor was 5 cm and the diameter was 4 cm. The reactor was cooled by circulating tap water inside the cooling jacket around the reactor. The temperature inside the reactor was monitored with a waterproof DS18B20 Digital Temperature sensor which was connected to an Arduino Uno. After the reactor, the liquid and the gas were separated in the glass separation unit by passing the aerosol through a filter (glass frit).

The outlet gas was passed through a pressure safety valve that opens at 0.5 bar to ensure that no pressure build-up can occur in the reactor and the separation unit. Then, the gas flowed into a glass silica dryer which contained silica gel granulates with a diameter of 1 to 3 mm (Merck) in order to collect the remaining MEA in the gas. The ExplorIR®-M-100 $CO_2$ sensor (Angst+Pfister Sensors and Power, Germany) coupled with a software from the same company were used to measure the $CO_2$ concentration at the outlet. The $CO_2$ sensor had an accuracy of ±300 ppm plus 5% of the reading. Corrosion-resistant materials which were compatible with MEA such as polyamide tubing and stainless steel valves were used in the set-up.

The $CO_2$ and the $N_2$ gases were thoroughly blown through the reactor while starting the experiments. The $CO_2$ percentage in the gas at the end of the reactor was recorded throughout the experiment. To ensure safety and the consistency of the measurements, MEA was sprayed to the reactor after the same $CO_2$ concentration at the inlet and outlet of the reactor were observed. The set-up was cleaned by pumping water after the experiments.

The temperature of the reactor was monitored with a thermometer inserted inside the reactor. The absorption process is exothermic, so cooling water was circulated around the reactor to keep the reactor temperature stable. The temperature changed between 23 and 33ºC for the experiments with pure MEA. For lower MEA concentrations, it changed between 23 and 31ºC.

One data point (G = 3.1 $L \cdot min^{-1}$, L = 10 $ml \cdot min^{-1}$, 14% CO2, pure MEA) was repeated four times on different days. The standard deviation and 95% confidence interval were calculated for the absorption efficiencies and $K_G a$ values. The 95% confidence interval was 0.59% for the absorption efficiency and 0.31 $kmol \cdot m^{-3} \cdot kPa^{-1} \cdot h^{-1}$ for the $K_G a$. The error bars in all the graphs show a 95% confidence interval on both sides. Six other data points were repeated twice on different days. The differences in these data were in the error range.

Graphs of the results were depicted in MATLAB 2020b. Process flow chart of the reactor system used in this work and the process flow chart of the whole $CO_2$ capture plant were depicted in Inkscape.

### 2.4. NMR analysis

$^{13}$C-NMR spectra is used to detect inorganic carbon species in solutions. It was used to explain the carbon capture mechanism into amines [35,36]. $^{13}$C-NMR spectra were carried out at room temperature on a 400 MHz Varian Inova spectrometer equipped with a 5 mm OneNMR PFG probehead. The samples were measured without addition of a deuterated solvent. The chemical shift scale ($\delta$) was calibrated relative to the methanol peak (49.5 ppm) in $D_2O$. Free induction decays were collected with a 75° pulse of 9.0 µs, a spectral width of 28 kHz, an acquisition time of 1.0 s, a preparation delay of 30 s (> 5 times the longest $T_{1C}$) and 100 accumulations. A line-broadening factor of 2 Hz was applied before Fourier transformation to the frequency domain.

### 2.5. Computational methods for the interaction between the parameters

The interaction between the parameters was checked by using the ANOVA test. The test was executed using *f_regression* function deployed in scikit-learn (version 0.24.2) utilizing Conda package management and Python 3.7.4. The calculation was performed using the ANOVA test. Beside the process variables, polynomial and rational interaction between these variables have been computed. The maximum total degree of the polynomial was set to 3 and the maximum degree that each variable can have within the polynomial was set to 2. The same rule is valid for the numerator and denominator of the rational form.

## 3. Results and Discussions

### 3.1. Droplet size analysis

There are only a few studies in the literature which measured the droplets sizes for the $CO_2$ capture applications. There was a wide variation in reported droplet sizes which ranged from around 40 µm to a few millimeters since different nozzle types were used [8,37–39]. Some of these studies worked with water or NaOH solutions which have different physical properties than MEA [37,39]. Although the droplet sizes give an idea of what is expected when MEA is used, the actual droplet sizes can change significantly with changing viscosity, surface tension and density of the liquids and liquid flow rate.

Spraying pure MEA into air can be flammable. Therefore, in this study, water at various flow rates and aqueous PG solutions at various concentrations were sprayed. Concentrations of PG solutions were selected so that they had similar surface tensions and viscosities to MEA. Viscosities and surface tensions of pure MEA and aqueous PG solutions were measured. The results were in line with the literature data (Fig. A.1 and Fig. A.2.) In addition, pure water was also sprayed at different flow rates in order to check for the effects of liquid flow rate on droplet sizes and interfacial areas. An empirical correlation by Ramisetty et al. [40] predicts droplet diameter based on liquid flow rate, frequency and intensity of the ultrasound and physical properties of the liquid such as viscosity, surface tension and density [40]. This correlation was first fitted, verified and then employed to reasonably predict the pure MEA droplet sizes. Fitting was done using the measured Sauter mean droplet diameter (D32) of water at various flow rates and PG at various weight percentages. The details of the calculations were given in the Appendix. The fitted correlation was able to predict D32 with less than 30% error (Table 1). A comparison between the predictions by the empirical correlation and the experimental values is shown in Fig. A.3. The droplet sizes of pure MEA were calculated with the same empirical equation [40]. The droplet sizes are expected to be between 75.0 and 108 μm (Table 1). At the same liquid flow rate (10 $ml \cdot min^{-1}$), the droplet size decreased from 108 to 85.4 μm when MEA wt.% increased from 30 to 100%. The number- and volume-weighted probability density distributions were given for water and PG in Figure 3 a-d. If the nozzle cannot break down the liquid into droplets properly, most of the liquid will be carried out in a few large droplets. Such poor atomization decreases interfacial area. If this is the case, peaks outside the nicely distributed curves are expected to occur especially in volume-weighted probability density distributions. The areas under the curves were one for all the parameters tested. Since the droplet sizes are properly distributed without any unexpected peaks at large droplet sizes, it can be concluded that the quality of the atomization was not compromised even at high viscosities.

Table 1. Droplet sizes of water, aqueous PG and MEA solutions at various concentrations and flow rates. MEA was not sprayed (The abbreviation, n.a., means not analyzed). The values corresponding to MEA were calculated based on the results of water and PG.

| **No** | **Component** | **wt. %** | **Flow rate (ml·min$^{-1}$)** | ***γ*** **(mN.m$^{-1}$)** | ***μ*** **(cP)** | ***ρ*** **(kg. m$^{-3}$)** | ***D32*** **(μm)-experimental** | ***D32*** **(μm) - calculated from** [40] | **Error %** |
|---|---|---|---|---|---|---|---|---|---|
| 1 | Water | 100 | 5 | 72.0 | 1.00 | 1000 | 77.3 | 106 | 27 |
| 2 | Water | 100 | 10 | 72.0 | 1.00 | 1000 | 91.0 | 121 | 25 |
| 3 | Water | 100 | 20 | 72.0 | 1.00 | 1000 | 112 | 138 | 18 |
| 4 | PG | 16 | 10 | 60.0 | 1.50 | 1005 | 94.1 | 116 | 19 |
| 5 | PG | 25 | 10 | 55.0 | 2.00 | 1008 | 98.4 | 113 | 13 |
| 6 | PG | 35 | 10 | 50.0 | 2.70 | 1011 | 101 | 109 | 7.2 |
| 7 | PG | 48 | 10 | 45.0 | 4.00 | 1015 | 103 | 105 | 2.3 |
| 8 | PG | 86 | 10 | 40.0 | 22.0 | 1028 | 73.5 | 87.3 | 16 |
| n.a. | MEA | 30 | 10 | 59.6 | 2.99 | 1010 | n.a. | 108 | n.a. |
| n.a. | MEA | 100 | 5 | 47.5 | 25.5 | 1032 | n.a. | 75.0 | n.a. |
| n.a. | MEA | 100 | 10 | 47.5 | 25.5 | 1032 | n.a. | 85.4 | n.a. |
| n.a. | MEA | 100 | 20 | 47.5 | 25.5 | 1032 | n.a. | 97.2 | n.a. |

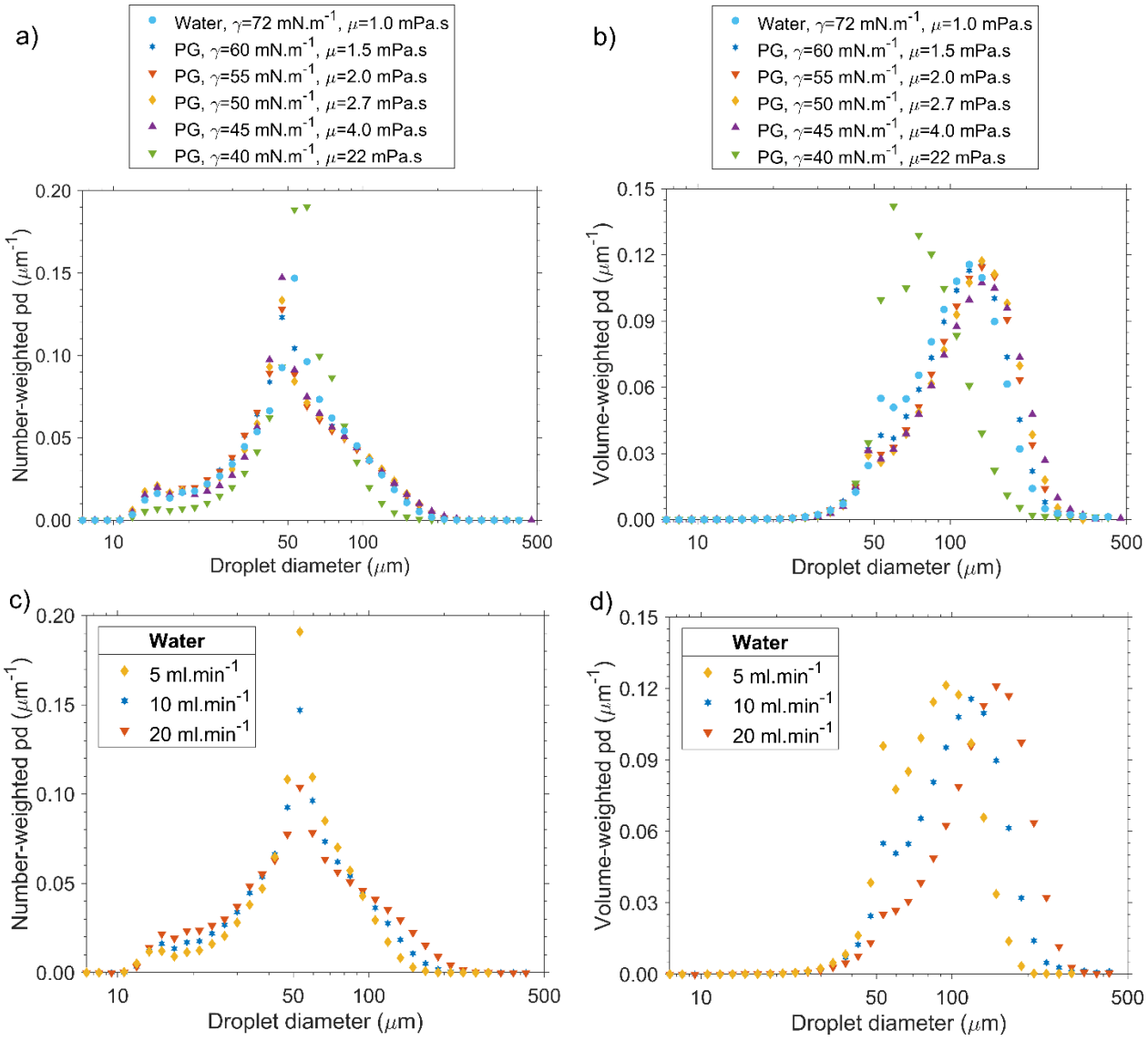


Figure 3. Probability density (pd) distributions. a) Number-weighted pd of water and PG at various surface tensions and viscosities, b) volume-weighted pd of water and PG at various surface tensions and viscosities, c) number-weighted pd of water at several flow rates, d) volume-weighted pd of water at several flow rates. The x-axes are in log scale.

Droplet sizes define the diffusion path. In our previous work [41], we provided a simple solution of the convection-diffusion equation to calculate the critical droplet diameter where the mass transfer limitations start. In order to have no mass transfer limitations, the time it takes for $CO_2$ concentration to

reach from zero to 99% of the solubility (Eq. (1)) needs to be less than the characteristic reaction time [41]. For fast reactions such as absorption of $CO_2$ into MEA, the characteristic reaction time approaches zero, forcing the desired droplet diameter also towards zero. Nozzles that can generate very fine droplets usually have low aerosol volume concentrations. As a result, the total amount of chemical absorbent per gas molecules decreases. Therefore, mass transfer limitations are difficult to completely avoid for the absorption of $CO_2$ into MEA by adjusting the droplet sizes. In this case, droplet size gains importance since it is related to the interfacial area.

$$t_{99} = 0.14\frac{D^2}{D_{CO2}} \tag{1}$$

where $t_{99}$ is the time it takes for the $CO_2$ concentration to rise from 0 to 99% of the solubility (s), $D$ is the droplet diameter (m) and $D_{CO2}$ is the diffusion coefficient of $CO_2$ ($m^2.s^{-1}$).

Since absorption of $CO_2$ into MEA is extremely fast, the reaction is taking place in the liquid film. As a result, interfacial area for mass transfer and available free MEA amount at the interface determine how much $CO_2$ is going to be absorbed. When conventional 30 wt.% MEA is used, water molecules occupy a large fraction at droplet surface. When MEA concentration is increased, there are more MEA molecules at the interface. Therefore, increasing the MEA concentration can increase the total amount of $CO_2$ captured. To capture more $CO_2$ per MEA molecules, either interfacial area or circulation inside the droplets need to be increased. It is not possible to characterize circulation inside the droplet in this system and its effects on $CO_2$ absorption rate. However, interfacial area can be calculated theoretically from the results of the image analysis.

Aerosol number concentrations were reported in every 3 mm inside the spray for PG at various surface tensions and viscosities and for water at various flow rates in Fig. A.4 a and b, respectively. Average aerosol number concentrations and interfacial areas of water at different flow rates and PG at different concentrations are given in Table 2. Interfacial surface area was calculated theoretically by multiplying aerosol number concentration with surface area of one droplet which was calculated by using the reported D32 values in Table 1.

Table 2. Aerosol number concentration and predicted interfacial area of water at various flow rates and aqueous PG at various concentrations.

| **Chemical** | **wt. %** | **Flow rate ($ml \cdot min^{-1}$)** | **Average number concentration ($cm^{-3}$)** | **Interfacial area ($m^2.m^{-3}$)** |
|---|---|---|---|---|
| Water | 100 | 5 | 2371 | 83.7 |
| Water | 100 | 10 | 2704 | 124 |
| Water | 100 | 20 | 2511 | 150 |
| PG | 16 | 10 | 2577 | 109 |
| PG | 25 | 10 | 2586 | 104 |
| PG | 35 | 10 | 2396 | 89.4 |
| PG | 48 | 10 | 2318 | 80.3 |
| PG | 86 | 10 | 2928 | 70.1 |

Aerosol number concentration did not change much with increasing liquid flow rate. It even decreased when liquid flow rate was increased from 10 to 20 $ml \cdot min^{-1}$. However, droplet sizes increased significantly with increasing liquid flow rates. As a result, interfacial area increased with increasing liquid flow rates. PG solutions between 16 and 48 wt. % had relatively low viscosities but varying surface tension (Table 1). Interfacial area did not change significantly at these weight percentages. However, PG solution at 86 wt.% had a significantly lower interfacial area. It seems that the effect of viscosity on D32 and, as a result, on interfacial area starts to become significant at viscosities as high as 22 cP, which is similar to the viscosity of pure MEA. Average aerosol number concentration for water and PG were 2529±484 $cm^{-3}$ and 2561±400

$cm^{-3}$, respectively. When the average aerosol number concentration for PG solutions and the expected D32 of pure MEA (Table 1) were used, the interfacial area for MEA is expected to be 45.3, 58.7 and 76.0 $m^2 \cdot m^{-3}$ for pure MEA at 5, 10 and 20 $ml \cdot min^{-1}$ respectively. It is expected to be 93.8 $m^2 \cdot m^{-3}$ for 30 wt.% MEA at 10 $ml \cdot min^{-1}$.

### 3.2. Absorption experiments in a spray column

The system performance was assessed with absorption efficiency (Eq. (2)) and $K_G a$. $K_G a$ includes both gas phase and liquid phase resistances to mass transfer (Eq. (3)). $K_G a$ was calculated based on the two-film theory by Eq. (4) [2,9,11]. Pure MEA and 10 vol. % $CO_2$ were used in all the experiments unless otherwise stated.

$$absorption\ efficiency = \left(\frac{C_{CO_2,in} - C_{CO_2,out}}{C_{CO_2,in}}\right) \cdot 100\% \quad (2)$$

where $C_{CO2,in}$ and $C_{CO2,out}$ are the $CO_2$ molar concentration ($mol \cdot L^{-1}$) at the inlet and outlet of the reactor, respectively.

$$\frac{1}{K_G a} = \frac{1}{k_G a} + \frac{H}{k_L a \cdot E} \quad (3)$$

where $K_G a$ is the overall mass transfer coefficient ($kmol \cdot m^{-3} \cdot kPa^{-1} \cdot h^{-1}$), $k_G$ is gas side mass transfer coefficient ($kmol \cdot m^{-2} \cdot kPa^{-1} \cdot h^{-1}$), $a$ is the interfacial area for mass transfer ($m^2.m^{-3}$), $H$ is Henry's coefficient ($kPa.m^3.kmol^{-1}$), $k_L$ is liquid side mass transfer coefficient ($m \cdot h^{-1}$) and $E$ is the enhancement factor of the reaction

$$K_G a = \frac{G_{inert} \cdot (Y_{CO_2,in} - Y_{CO_2,out})}{Z \cdot P \cdot (y_{CO_2} - y^*_{CO_2})_{lm}} \quad (4)$$

where $G_{inert}$ is the inert gas velocity ($kmol.m^{-2}.h^{-1}$), $P$ is the total pressure (kPa), $Z$ is the height of the reactor (m), $Y_{CO2}$ the mole ratio of $CO_2$ in the gas phase, $y_{CO2}$ is the mole fraction of $CO_2$ in the gas phase and $y_{CO2}^*$ is the mole fraction of $CO_2$ in equilibrium with the liquid phase which is assumed to be zero due to the fast reaction between MEA and $CO_2$ [2]. The molar fractions equal to $CO_2$ partial pressure over the total gas pressure whereas the molar ratios are $CO_2$ molar fraction over $N_2$ molar fraction. The subscript *lm* denotes the logarithmic mean.

### 3.2.1. Effect of inlet $CO_2$ concentration

Increasing $CO_2$ concentration in the flue gas has a negative effect on both absorption efficiency and $K_G a$ as shown in Figure 4a and b, respectively. With increasing $CO_2$ concentration, concentration driving force increases. That is expected to result in a higher $CO_2$ transfer rate from the gas to the liquid. However, a higher $CO_2$ concentration leads to more $CO_2$ being present for the same amount of available MEA. In other words, the molar ratio of MEA to $CO_2$ decreased as $CO_2$ concentration increased. This results in less $CO_2$ being absorbed in proportion to the inlet $CO_2$ concentration. As a result, both absorption efficiency and $K_G a$ decreased with increasing $CO_2$ concentration. This effect indicates that the mass transfer performance is dominated by the liquid phase resistance. The same trend has also been observed previously [9]. The highest absorption efficiencies (88 – 98%) were observed when G/L ratio was the lowest at 10 ml·min$^{-1}$ liquid flow rate (i.e. G/L = 309). $K_G a$ values corresponding the same liquid flow rate and G/L ratio were also quite high ranging between 3.23 and 5.68 kmol·m$^{-3}$·kPa$^{-1}$·h$^{-1}$.

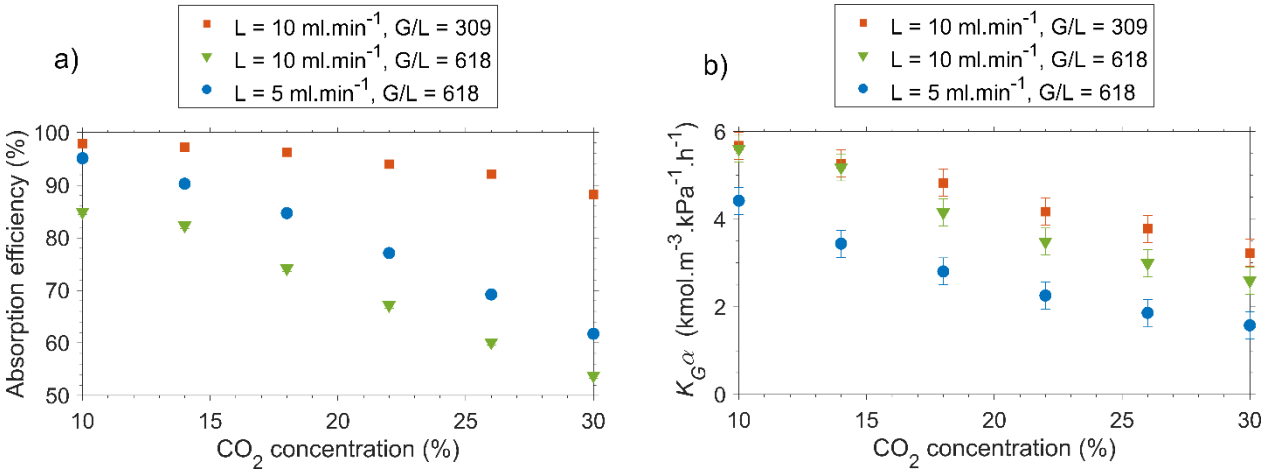


Figure 4. Effect of $CO_2$ concentration on a) absorption efficiency and b) $K_G a$ at different liquid flow rates (L) and gas to liquid volumetric flow rate ratio (G/L). Pure MEA was used.

At the same G/L ratio, lower liquid flow rate indicates a higher residence time for both liquid and gas phase. More $CO_2$ can be absorbed with higher residence time as shown in Figure 4a. However, $K_G a$ decreased at high residence times (Figure 4b). That indicates that most of the absorption took place in the

immediate vicinity of MEA injection. As the residence time increased, rate of absorption decreased but absorption efficiency increased.

### 3.2.2. Effect of gas flow rate

Increasing gas flow rate can increase chaotic advection in the gas phase. As a result, mass transfer rate might be enhanced by increasing gas flow rate if mass transfer is controlled by the gas phase resistance. In that case, absorption efficiency and $K_G a$ are expected to increase with increasing gas flow rate. However, that was only valid for $K_G a$ for a few data points. Increasing gas flow rate led to a decrease in the absorption efficiency at the same liquid flow rate (Figure 5a). $K_G a$ increased with increasing gas flow rate only when liquid flow rate was 20 ml·min$^{-1}$ and the gas flow rate was below 25 L·min$^{-1}$. At lower liquid flow rates, no significant change in $K_G a$ was observed with changing gas flow rates (Figure 5b). That is because increasing gas flow rates decreased the available MEA amount per $CO_2$ molecules at the same liquid flow rate. In the same manner, increasing liquid flow rate increased the available MEA amount at the same gas flow rate. Consequently, absorption efficiency increased with increasing liquid flow rate when gas flow rate was the same. Therefore, it seems that the gas phase controlled mass transfer takes place at low gas flow rates only. Kuntz and Aaronwilas also observed gas phase controlled mass transfer at low gas flow rates in a spray column [9]. In addition, in packed bed reactors, many researchers reported that $K_G a$ was unaffected by gas flow rate [13–17].

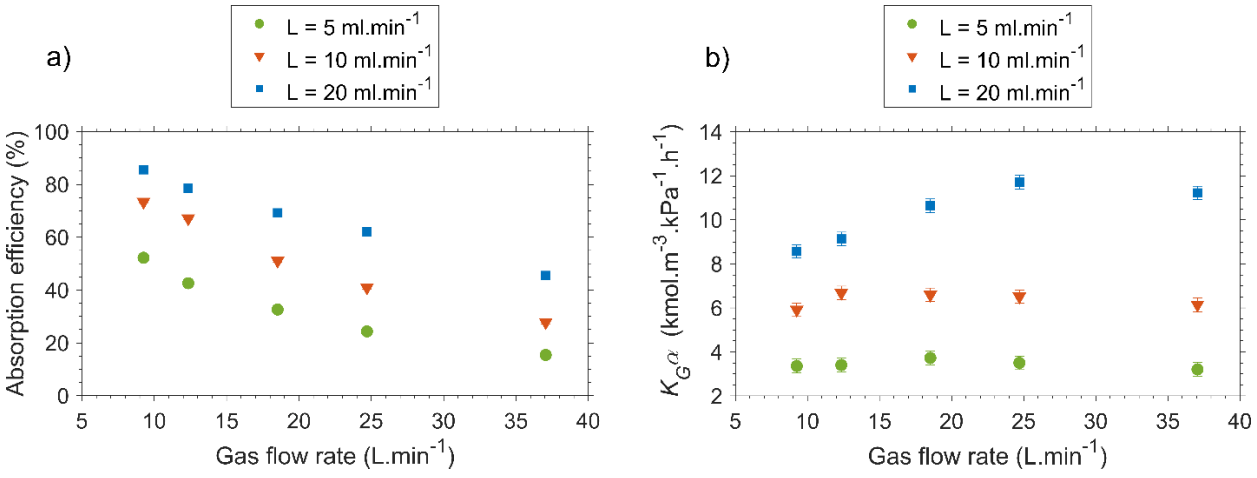


Figure 5. Effect of gas flow rate on a) absorption efficiency, b) $K_G a$ at different liquid flow rates (L). Pure MEA was used. The $CO_2$ inlet concentration was 10%.

### 3.2.3. Effect of liquid flow rate

As it can be seen from Figure 6a, the absorption efficiency increased as liquid flow rate increased at both gas flow rates. In addition, absorption efficiency was higher at the low gas flow rate. That is because, there were more available MEA per $CO_2$ molecules in that case. The increase in absorption efficiency was more rapid at lower liquid flow rates. As MEA to $CO_2$ molar ratio provided to the reactor was increased, the rate of increase in absorption efficiency reached a plateau. $K_G a$ also increased as liquid flow rate increased (Figure 6b). That is because available surface area was increased as liquid flow rate increased as discussed previously (Table 2). The same phenomenon was also observed both in spray and packed columns [9,11–17]. These studies also associated the increase in liquid flow rate to the increase in interfacial area [9,11–17].

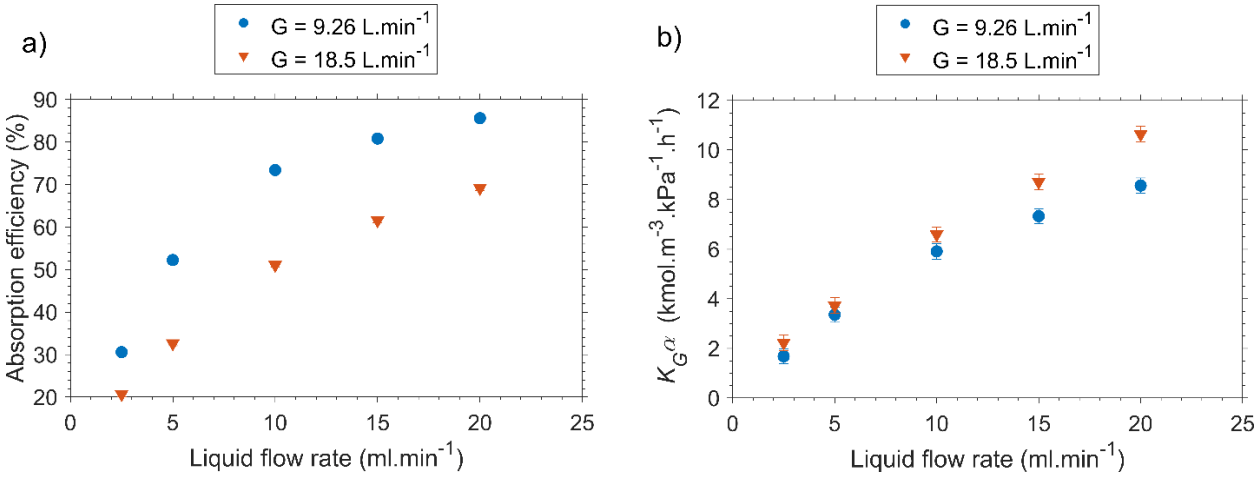


Figure 6. Effect of liquid flow rate on a) absorption efficiency, b) $K_G a$. G is the gas flow rate at different gas flow rates (G). Pure MEA was used. The $CO_2$ inlet concentration was 10%.

### 3.2.4. Effect of MEA concentration

Effects of MEA concentration on absorption efficiency and $K_G a$ are shown in Figure 7a and b, respectively. Absorption efficiency increased with increasing MEA concentration. Almost all $CO_2$ is absorbed at high MEA concentrations when liquid flow rate was 10 ml·min$^{-1}$ and G/L was 276. $K_G a$ value was not affected significantly with increasing gas flow rate as it can be seen from the results when liquid flow rate was 10 ml·min$^{-1}$ and gas flow rate was doubled. This indicates that liquid resistance controls the mass

transfer. $K_G a$ increased significantly at high MEA concentrations when liquid flow rate was doubled at the same G/L ratio since interfacial area is also increased with liquid flow rate. Increase in $K_G a$ with increasing absorbent concentrations were observed before, as well [9,11–17], but none of the studies used pure MEA.

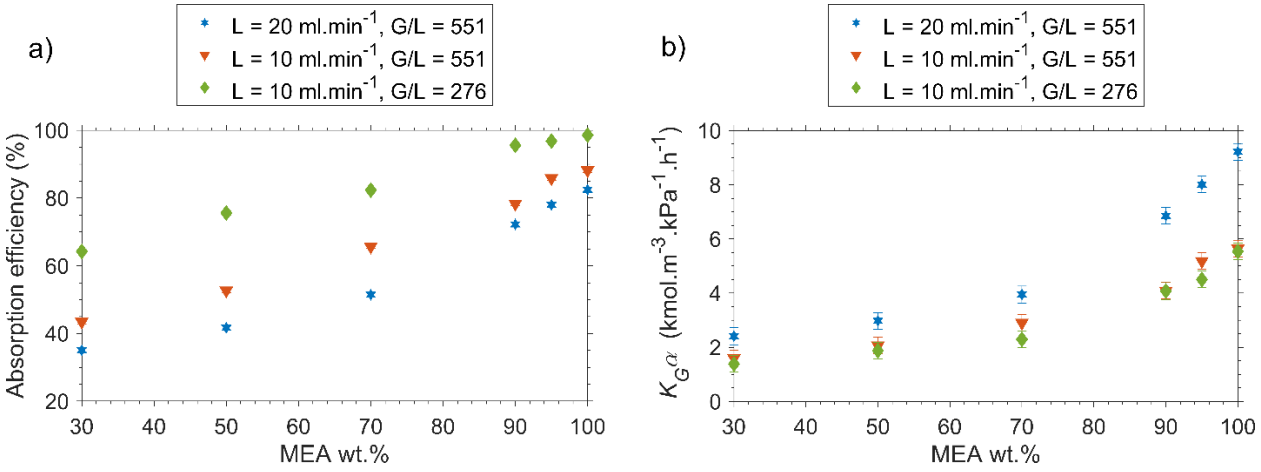


Figure 7. Effect of MEA concentration on a) absorption efficiency, b) $K_G a$ at different liquid flow rates (L) and gas to liquid volumetric flow rate ratio (G/L). The $CO_2$ inlet concentration was 10%.

### 3.2.5. Effect of stoichiometric ratio of MEA to $CO_2$

The interdependence of the parameters makes it quite difficult to isolate the most significant operational parameters. Changing gas and liquid flow rates change both molar inlet ratios of MEA to $CO_2$ (the stochiometric ratio) and residence times. In addition, gas and liquid flow rates might affect mass transfer rates by changing hydrodynamic conditions around and inside droplets. Most probably due to the abundance of interrelated parameters, the stochiometric ratio has not been studied as a parameter in $CO_2$ capture applications. In addition, some nozzles such as pneumatic nozzles require a fixed gas to liquid ratio for proper atomization. Therefore, it is not possible to study the effect of stochiometric ratio in some setups due to the technical limitations. Ultrasonic nozzles do not require a certain gas to liquid ratio which enabled us to see the effect of the stochiometric ratio. In this work, we selected the experimental data points such that they all had similar stoichiometric ratios. According to the zwitterion mechanism, molar ratio of MEA to $CO_2$ was two [42,43] when MEA acts as a base. Most of the data points studied in this work had a stoichiometric ratio of two or higher. Effect of the stoichiometric ratio on absorption efficiency and $K_G a$ are shown in Figure 8 a and b, respectively. More detailed graphs on the effects of stoichiometric ratio are given

in Appendix A.4. The stoichiometric ratio was changed either by changing the $CO_2$ inlet concentration (Fig. A.5), gas flow rate (Fig. A.6), liquid flow rate (Fig. A.7) or MEA concentration (Fig. A.8).

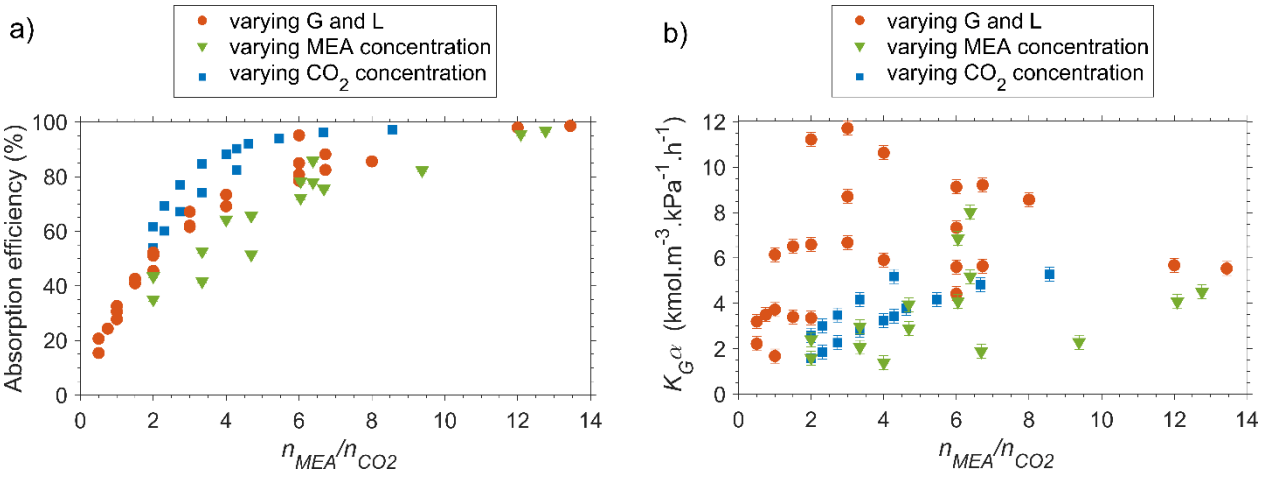


Figure 8. Effect of the stoichiometric ratio on a) absorption efficiency, b) $K_Ga$.

Effect of stoichiometric ratio along with gas ($CO_2$) and liquid (MEA) concentrations are the most important parameters that determine the absorption efficiency. In most $CO_2$ capture applications, the inlet $CO_2$ concentration does not change much and MEA concentration is fixed. Thus, it is important to check the effect of the stoichiometric ratio in the specific absorption columns if a certain outlet $CO_2$ concentration is desired due to the regulations on $CO_2$ release.

If absorption efficiency is known, the outlet $CO_2$ concentration can be predicted. $K_Ga$ has a linear dependence on gas flow rate and has both a linear and logarithmic dependence on the difference in $CO_2$ inlet and outlet concentrations as shown in Eq (4). Because of the logarithmic dependence, small differences in outlet $CO_2$ concentration might lead to large changes in $K_Ga$. That seems to result in great variation in $K_Ga$ based on the stoichiometric ratio. It is interesting to see that while absorption efficiency is largely influenced by the stoichiometric ratio, $K_Ga$ is not affected much by the stoichiometric ratio. $K_Ga$ is mostly determined by liquid flow rate since liquid flow rate changes interfacial area as it has been discussed in the previous sections and evidenced further in Fig.A.6. It seems that prediction of $K_Ga$ based on these parameters requires more advanced computational pattern recognition tools such as artificial intelligence techniques.

### 3.2.6. Interaction between the parameters

In this work, we reported the effects of operational parameters by keeping other parameters at several levels. For example, we checked the effects of MEA concentration at different liquid flow rates and at different gas to liquid volumetric flow rate ratio. Therefore, we were able to check the interactions between the parameters by calculating the p-values in the analysis of variance (ANOVA) test.

To calculate the statistical significance of each input variable (i.e. liquid flow rate, gas flow rate, MEA concentration and $CO_2$ concentration) on the output of the system (i.e. $K_G a$), p-values between the input and process variables were calculated. The p-value measure the statistical significance of a variable over another variable. The lower the p-value is, the more effect the input variable has on $K_G a$. Conventionally, the value of 0.05 has been chosen as threshold over which two variable has a weak interdependence [44]. The total amount of variables and combinations of variables which have p-values smaller than 0.05 was 189. The first 10 variables that have lowest p-values in the ANOVA test are shown in Table 3. As it can be seen from Table 3, most of the variables are interdependent and almost all the terms contain L. In addition, first 9 terms contain forms of $L \cdot w_{MEA}$. These results are in line with our conclusions. Liquid flow rate makes a large difference in $K_G \alpha$ since it changes the interfacial area and the availability of MEA molecules per gas molecule. In addition, weight fraction of MEA has a large influence on $K_G \alpha$. The stoichiometric ratio of MEA to $CO_2$ is expected to approach to two when water is not present as discussed further in the next section [20]. Therefore, the second term in the table involves a term that is close to the stoichiometric ratio of MEA to $CO_2$. The gas flow rate appears later in the table and it always appears along with the liquid flow rate. We showed in the previous sections that the gas flow rate alone did not have a significant effect on $K_G \alpha$.

Table 3. Top 10 variables with the lowest p-values obtained in the ANOVA test. There were 189 parameters which has p-values lower than 0.05.

| ID | Parameter | p-value |
|---|---|---|
| **1** | $L \cdot w_{MEA}^2$ | 3.76e-33 |
| **2** | $L \cdot \frac{w_{MEA}^2}{y_{CO_2,in}}$ | 8.38e-33 |
| **3** | $L \cdot w_{MEA}$ | 4.21e-30 |
| **4** | $L^2 \cdot w_{MEA}^2$ | 4.21e-30 |
| **5** | $L^2 \cdot w_{MEA}$ | 1.21e-25 |
| **6** | $G \cdot L^2 \cdot w_{MEA}$ | 1.31e-21 |
| **7** | $G \cdot L \cdot w_{MEA}^2$ | 9.77e-21 |
| **8** | $\frac{y_{CO_2,in}}{L \cdot w_{MEA}}$ | 4.95e-20 |
| **9** | $L \cdot G \cdot w_{MEA}$ | 8.50e-20 |
| **10** | $\frac{L}{y_{CO_2,in}}$ | 5.48e-19 |

### 3.2.7. Mechanism of $CO_2$ capture into MEA at different weight fractions and into pure MEA at different $CO_2$ loadings

Three reaction mechanisms of $CO_2$ absorption in aqueous solutions of MEA were proposed so far [45]: zwitterion mechanism [42,43], thermomolecular mechanism [46,47], and base-catalyzed hydration mechanism [48]. Xie et al. showed by molecular modelling that a two-step mechanism which proceeds via a zwitterion intermediate to form carbamate is the most thermodynamically favorable route [49]. Indeed, the commonly accepted mechanism for $CO_2$ capture with primary, secondary and sterically hindered amines is the zwitterion mechanism which was initially proposed by Caplow [43] and reintroduced by Danckwerts [42]. In this mechanism, first, zwitterion is formed as an intermediate by the reaction between $CO_2$ and an amine (Eq. (5)**Error! Reference source not found.**). Then, the zwitterion undergoes deprotonation by a base

such as an amine, $OH^-$ or $H_2O$, resulting in the formation of carbamate as shown in Eq. (6) **Error! Reference source not found.** [2,35,50].

$$CO_2 + RNH_2 \leftrightharpoons RNH_2^+COO^- \quad (5)$$

$$RNH_2^+COO^- + RNH_2 \leftrightharpoons RNHCOO^- + RNH_3^+ \quad (6)$$

In aqueous solutions of MEA, $CO_2$ reacts with water to form carbonic acid ($H_2CO_3$) which, in turn, dissociates to form hydrogen ($H^+$), bicarbonate ($HCO_3^-$) and carbonate ions ($CO_3^{2-}$) as amine is consumed and pH decreases. Although there are some differences in the reaction pathways depending on the MEA concentration and $CO_2$ partial pressure, carbamate formation seems to be the main reaction mechanism in $CO_2$ absorption at high amine concentrations in water-lean solvents, as well [20,51]. The stoichiometric ratio of $CO_2$ to amine approaches to 1:1 in aqueous MEA solutions since water can also act as a base whereas the stoichiometric ratio approaches 1:2 when MEA acts as a base [20]. Therefore, the shift in stoichiometric ratio was expected although the exact MEA concentration where this occurs was not known.

The heat of absorption of MEA-based water-lean solvents was also found to be similar to the one in aqueous solvents [25]. Heat of absorption depends largely on the carbamate formation since this bond needs to be broken down during the desorption process. A 30 wt.% MEA in water-lean solvents is often used. The mechanism of $CO_2$ absorption into high MEA concentrations still needs be investigated.

In this work, we measured $^{13}$C-NMR spectra of the samples. A sample spectra is shown in Figure 9. All ppm values and the corresponding peak intensities are given in Table 5. The $^{13}$C-NMR spectra of all the samples are given in Fig A.9 and Fig. A.10. We obtained the $^{13}$C-NMR spectra of 30, 50, 70, 90 and 100 wt.% MEA at $CO_2$ loadings of around 0.1 mol $CO_2 \cdot mol^{-1}$ MEA. We observed carbamate formation in all the samples. Selecting similar loadings at different MEA concentrations enabled us to see the effect of MEA concentration on carbamate formation. Carbamate concentration stayed at similar levels up to 70 wt.% MEA. There was a significant increase in carbamate formation when 90 wt.% MEA and pure MEA were used. In fact, the intensity of the peaks that correspond to carbamate formation almost doubled at the same $CO_2$ loading when MEA concentration was increased from 70 to 90 wt.%. Therefore, the desorption energy requirement is expected to increase when 90 wt.% MEA is used.

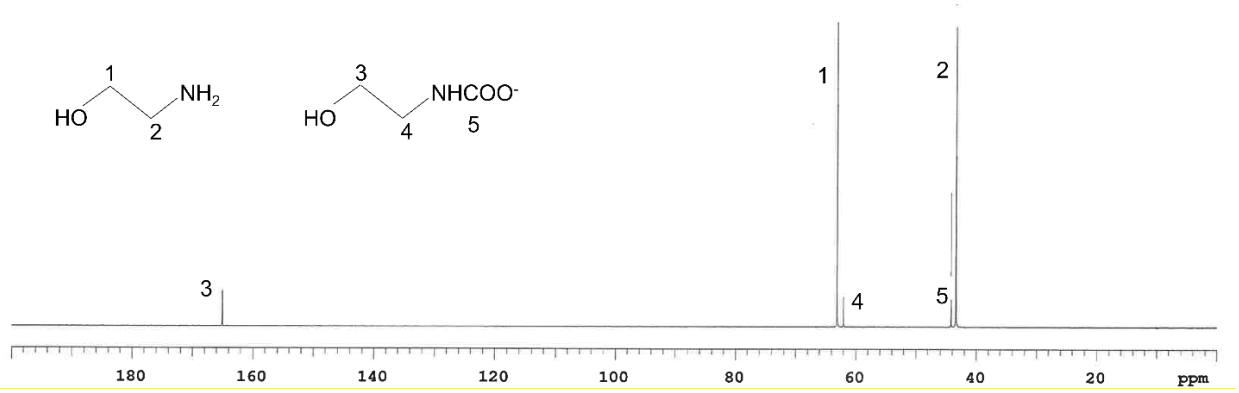


Figure 9. A sample NMR spectra of CO2 loaded MEA (50 wt.% MEA, pH=11.33) and the molecular structure in MEA-$CO_2$ system. Peak numbers are numbered according to the molecular bonds.

Table 4. Results of $^{13}$C-NMR spectra of $CO_2$-loaded MEA at different MEA wt. % and $CO_2$ loadings

| ID | MEA wt.% | $CO_2$ loading (mol $CO_2$ . mol MEA -1) | pH | Peak number 1 | Peak number 2 | Peak number 3 | Peak number 4 | Peak number 5 |
|---|---|---|---|---|---|---|---|---|
| 1 | 30 | 0.16 | 10.74 | 21.32 | 20.70 | 5.19 | 5.46 | 5.44 |
| 2 | 50 | 0.08 | 11.33 | 40.30 | 38.70 | 4.23 | 4.29 | 4.02 |
| 3 | 70 | 0.11 | 11.20 | 56.47 | 54.31 | 5.54 | 5.63 | 5.59 |
| 4 | 90 | 0.11 | 11.69 | 61.10 | 60.47 | 12.93 | 12.87 | 12.71 |
| 5 | 100 | 0.11 | 11.97 | 69.95 | 67.58 | 12.82 | 13.08 | 12.89 |
| 6 | 100 | 0.18 | 11.53 | 58.78 | 57.24 | 20.22 | 20.27 | 19.76 |
| 7 | 100 | 0.27 | 11.03 | 54.33 | 52.78 | 23.44 | 23.99 | 23.99 |
| 8 | 100 | 0.33 | 10.74 | 51.51 | 50.22 | 25.84 | 26.14 | 25.47 |

We also measured the $^{13}$C-NMR spectra of pure MEA at different $CO_2$ loadings (Table 4, ID=3-8). Increasing $CO_2$ concentration leads to a decrease in pH levels. As the $CO_2$ loading increased, the carbamate formation is increased, as expected. Hydrolysis of carbamate and formation of bicarbonate have not been

observed in any of the samples. Lv et al. [35] found that hydrolysis of carbamate was only observed at $CO_2$ loadings around 0.4 mol $CO_2$ · mol MEA at 30 wt.% MEA. In addition, the authors found that carbamate was formed though the reaction of $CO_2$ and MEA at low $CO_2$ loadings whereas, at high $CO_2$ loadings, $CO_3^-$ / $CO_3^{2-}$ reacted with MEA to form carbamate [35]. Increased carbamate formation at high $CO_2$ loadings due to the reaction between the reaction of MEA and $CO_3^-$ / $CO_3^{2-}$ might lead to higher regeneration energy. Hydrolysis of carbamate and formation of bicarbonate were eliminated in non-aqueous solvents [51]. Hydrolysis of carbamate is not expected in pure MEA. Therefore, our results are in line with the literature findings. However, we demonstrated that similar levels of carbamate was formed for MEA concentrations up to 70 wt.%. Carbamate levels increased significantly above 90 wt. %. As long as the carbamate formation stays at similar levels, the desorption of $CO_2$ from MEA should results in similar heat of desorption.

### 3.2.8. Comparison to literature data

$K_Ga$ is often used to compare the performance of absorption columns. $K_Ga$ of several literature studies are compared to this work in Table 5. Most of $CO_2$ capture applications have $K_Ga$ around or below 2 $kmol \cdot m^{-3} \cdot kPa^{-1} \cdot h^{-1}$. Only three applications were found have a higher $K_Ga$ than that, of which two are packed columns. They have structured packing and a relatively small reactor volume. This indicates that currently most spray columns lack in performance. To the best of our knowledge, the highest $K_Ga$ in the literature was found as 6.05 $kmol \cdot m^{-3} \cdot kPa^{-1} \cdot h^{-1}$ in a spray column. We achieved a $K_Ga$ of 11.7 $kmol \cdot m^{-3} \cdot kPa^{-1} \cdot h^{-1}$ when liquid flow rate was 20 $ml.min^{-1}$ and gas flow rate was 25 $L.min^{-1}$. This value is significantly higher than all other literature values. This means that the column length can be reduced to almost its half compared to the highest value obtained in literature. Among these studies, the highest MEA concentration was 55 wt. %. $K_Ga$ of this work was 0.58 $kmol \cdot m^{-3} \cdot kPa^{-1} \cdot h^{-1}$ [14]. This value was significantly lower than $K_Ga$ values found in this paper with pure MEA. Even with 30 wt.% MEA, we obtained $K_Ga$ as 2.41 $kmol \cdot m^{-3} \cdot kPa^{-1} \cdot h^{-1}$, which is also higher than most of the literature values.

Table 5. Comparison of $K_G a$ values of spray and packed bed absorption columns. Abbreviation "n.s." means not specified.

| **Absorption column** | **Nozzle or packing type** | **Solvent** | **wt. %** | **Reactor volume (L)** | **Gas flow rate ($L \cdot min^{-1}$)** | **Liquid flow rate ($L \cdot min^{-1}$)** | **Inlet $CO_2$ concentration (%)** | **$CO_2$ loading (mol $CO_2 \cdot mol^{-1}$ MEA)** | **$K_G a$ ($kmol \cdot m^{-3} \cdot kPa^{-1} \cdot h^{-1}$)** | **Reference** |
|---|---|---|---|---|---|---|---|---|---|---|
| Spray column | Ultrasonic nozzle | MEA | 100 | 0.06 | 24.7 | 0.02 | 10 | 0.00 | 11.7 | This work |
| Spray column | Impingement nozzle | MEA | 30[a] | 4.32 | 50.0[b] | 1.35[b] | 15[a] | 0.00 | 6.05 | [9] |
| Packed column | Sulzer EX | NaOH[a] | 4 | 0.50 | 4.93 – 10.4[b] | 0.05[b] | 1 | n.s. | 4.00 | [13] |
| Packed column | Sulzer DX | MEA | 18[a] | 0.63 | 5.66[b] | 0.05[b] | 10 | 0.00 | 3.00 | [52] |
| Spray column | Pressure swirl nozzle | MEA | 30 | 3.19 | 320[a] | 1.14[a] | 12 | 0.00 | 1.70[a] | [38] |
| Packed column | Gempak 4A | MEA | 37[a] | 18.8 | 107[b] | 0.97[b] | 14.9 | 0.00 | 1.20 | [14] |
| Packed column | 16 mm Pall rings | MEA | 43[a] | 18.8 | 170[b] | 1.77[b] | 15 | 0.23 | 0.61 | [14] |
| Packed column | IMTP-15 | MEA | 55[a] | 18.8 | 107[b] | 0.97[b] | 15 | 0.22 | 0.58 | [14] |
| Packed column | Gempak 4A | MEA | 18[a] | 17.4 | > 113[b,c] | 2.00[b] | < 15 | 0.00 | 1.20 | [53] |
| Packed column | Gempak 4A | MEA | 18[a] | 17.4 | > 113[b,c] | 3.00[b] | < 15 | 0.31 | 0.90 | [53] |
| Packed column | Sulzer EX | AMP | 27[a] | 0.50 | 4.89 – 10.3[b] | 0.05[b] | n.s. | 0.10 | 1.15 | [15] |
| Packed column | Sulzer EX | MEA | 30[a] | 1.04 | 10.4[b] | 0.04[b] | 15[a] | 0.30 | 0.80 | [17] |
| Packed column | Sulzer EX | DEEA | 37[a] | 1.04 | 9.28[b] | 0.04[b] | 3[a] | 0.09-0.11 | 0.22 | [17] |

| | | | | | | | | | | |
|---|---|---|---|---|---|---|---|---|---|---|
| Packed column | Sulzer EX | AMP | 10[a] | 0.50 | 5.32[b] | 0.05[b] | 7[a] | 0.15 | 0.60 | [13] |
| Diameter varying spray column | Two impingement nozzles | MEA | 30 | 12.7 | 83.3[a] | 1.33[a] | 8 | 0.00 | 0.57 | [54] |
| Vortex flow spray column | Pressure swirl nozzle | NaOH | 5[a] | 5.11 | 400 | 3.00 | 3 | 0.00 | 0.30[a] | [19] |
| Packed column | Structured packing | $NH_3$ | 1 [a] | 42.4 | 500[b] | 11.5[b] | 3[a] | 0.00 | 0.25 | [16] |

*a: Unit conversion*

*b: Flow rate was calculated from flux*

*c: Inert gas flow rate were reported and $CO_2$ concentration was not specified. Therefore, exact gas flow rate is unknown.*

In this work, the droplet size analysis was performed at several positions inside the spray cone. We selected the column diameter based on the spray cone. Therefore, no dead zones at the sides are expected and not too many droplets stick on the walls of the column. In most spray column applications, the droplet analysis data are not available and the spray cone is not taken into account while designing the column. Therefore, not only increasing the absorbent concentration but also a careful selection of the operational parameters and the design of the absorber column played a significant role in obtaining a high $K_G a$.

### 3.2.9. Effects of using pure MEA on the economics of the overall process

#### 3.2.9.1. Adjustments to the current absorption-desorption process

Process flow diagram of a typical $CO_2$ capture process which utilizes absorption and desorption columns is given in the literature [4,50]. The $CO_2$ capture process using pure MEA in a spray column can be similar to a commercial amine-based post-combustion $CO_2$ capture process. The possible adjustments to the conventional set-up is shown in Figure 10 when pure MEA is used. A water-wash unit is employed after the packed absorption column to capture MEA in the vapor phase and recycle it back to the absorption column. In $CO_2$ capture plants, some of the stream coming from the water-wash section is injected back to the absorption column to recycle some of the MEA. However, MEA is highly diluted after washed with water. If $CO_2$ capture either with pure MEA or with highly concentrated MEA solutions is aimed, dilution of MEA with water needs to be avoided. Therefore, a small part of the water-wash section can be injected to the stripping column instead of the absorption column to gain MEA from the water-wash section. The lean MEA coming out of the desorption column is sent back to the absorption column. Sending a small part of the water-wash might increase the reboiler heat duties. However, we expect that will be minimal since 70% water in MEA solution coming out of the absorption column will be reduced to zero. However, for desorption with steam, some water still needs to be boiled in the reboiler. This steam will be cooled down in the condenser at the top of the desorption column. Then, it can be mixed with the pure MEA coming out of the main heat exchanger and aqueous MEA coming out of the water-wash section. In this way, pure MEA is diluted with aqueous MEA to some degree before entering the desorption column. MEA can be separated from water at the reboiler and sent back to the absorption column. In this configuration, all the water in the solution is boiled in the reboiler to provide steam for desorption. Therefore, the water amount can be reduced as much as

possible to reduce the heating duties. The amount of steam required depends on the total heat transfer area in the stripping column. Alternatively, microwave regeneration can be used to desorb $CO_2$ from pure MEA which has already been shown to work in aqueous MEA solutions up to 70 wt.% [55].

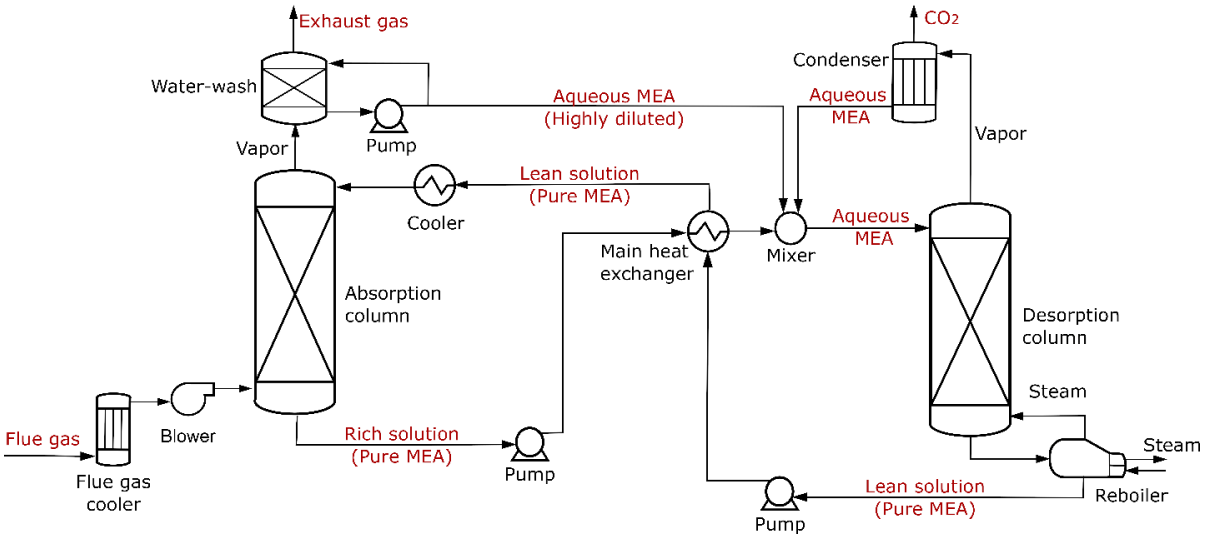


Figure 10. Prosses flow diagram of typical $CO_2$ capture process. Figure is adapted from [4,56]. There are two main differences in the process compared to the conventional ones reported in [4,56]. A small part of the outlet of the water-wash section which contains highly diluted aqueous MEA is fed to the line just before the desorption column instead of being fed to the line before the absorption column. The condenser outlet is fed is mixed with pure MEA coming out of the main heat exchanger before entering the desorption column.

#### 3.2.9.2. Simplified calculation of reboiler heat duty and discussions on capital costs

The effect of using pure MEA as a solvent is expected to reduce the equipment size and cost significantly when compared to a 30 wt.% amine-based capture process. As discussed in the previous section, we were able to achieve $K_G a$ values that are around 10 times higher than most literature values. This means that absorption column can be 10 times shorter. Therefore, the capital costs are also expected to decrease with the use of pure MEA. The energy requirement for the stripping section is the main cost item. Unlike the commercial process, the water is not pumped through the equipment and a minimal amount of water will be used in the desorption column. Consequently, steam and energy requirements of the entire process are also expected to be reduced if the desorption kinetics stays the same. In addition, parasitic losses are expected to decrease since less water will be vaporized in the desorption column. Below, we present a simplified calculation of regeneration heat duty at several MEA

concentrations. It should be noted here that the desorption rate from pure MEA solutions has not been studied. However, our $^{13}$C-NMR spectra results suggest that carbamate formation levels stays similar at the same $CO_2$ loadings up to  MEA at 70 wt.%.

Desorption of $CO_2$ from amines is an endothermic reaction. Desorption typically occurs around 120$^o$C [27]. A simplified analysis of the weight specific reboiler heat duty (eg. MJ/t $CO_2$) was done following the work of Oexman and Kather [56]. Reboiler heat duties of several water-lean solvents were calculated with the same approach in the work of Wanderley and Knuutila [27]. Regeneration energy ($Q_{regeneration}$) consist of sensible heat ($Q_{sensible}$), heat of desorption ($Q_{desorption}$) and latent heat of vaporization ($Q_{vaporization}$) (Eq. (7) - Eq. (9)). The sensible heat is the energy required to raise the temperature of the amine solution from the rich-lean heat exchanger to the reboiler temperature. The heat of desorption is the energy supplied to desorb $CO_2$ from the amine solutions. The latent heat corresponds to the energy required to evaporate water in the desorption column [56]. Among these heat expenditures of the reboiler, latent heat was found to play the most significant role [27].

$$Q_{regeneration} = Q_{sensible} + Q_{vaporization} + Q_{desorption} \tag{7}$$

$$Q_{sensible} = \frac{C_p(T_{reb} - T_{feed})}{\Delta q} \tag{8}$$

$$Q_{vaporization} = \Delta H_{vap,H2O} \frac{p_{H2O}}{p_{CO2}} \frac{1}{M_{CO2}} \tag{9}$$

$$Q_{desorption} = \frac{\Delta H_{des,CO2}}{M_{CO2}} \tag{10}$$

where $C_p$ is molar heat capacity (kJ·kg$^{-1}$·K$^{-1}$), $T_{reb}$ and $T_{feed}$ are the temperatures (K) in the reboiler and at the inlet of the desorption column (K), $\Delta q$ is the cyclic working capacity (kg $CO_2$ · kg$^{-1}$ solution) (Eqn. (11)), $M$ is molecular weight (kg.mol$^{-1}$), $\Delta H_{vap,H2O}$ is molar latent heat of water (kJ·mol$^{-1}$), $p_{H2O}$ and $p_{CO2}$ are the partial pressures of water vapor and $CO_2$ in the gas phase at the desorber outlet (kPa), $M_{CO2}$ is the molecular weight of $CO_2$ (kg·mol$^{-1}$) and $\Delta H_{des,CO2}$ is heat of desorption or absorption (kJ·mol$^{-1}$).

$$\Delta q = \Delta \alpha \frac{M_{CO2}}{M_{sol}} X_{MEA} \tag{11}$$

where $\Delta\alpha$ is the difference in rich and lean $CO_2$ loading (mol $CO_2$ · mol$^{-1}$ MEA), $M_{CO2}$ and $M_{soln}$ are the molecular weight of $CO_2$ and the solution (kg.mol$^{-1}$), $X_{MEA}$ is the molar fraction of MEA in the solution.

The heat of absorption of $CO_2$ from MEA is assumed to be 85 kJ·mol $CO_2^{-1}$ [57,58] $CO_2$ is assumed to be recovered at 100 kPa. The saturation pressure of water is 199 kPa at 120°C. The heat of absorption of $CO_2$ from MEA, desorption temperature and saturation pressure of water were assumed to be the same as in the work of Wanderley et al. [27]. Latent heat of water was 40.8 kJ·mol $H_2O$ [59]. The temperature of the stream coming out of the absorption column was assumed to be 50°C. Heat capacities of the MEA solutions at different weight percentages were obtained from the data presented by Weiland et al. [60]. The heat capacity at each MEA wt.% was averaged at $CO_2$ loadings of 0.05 and 0.4 mol $CO_2$ · mol MEA.

As it can be seen from Figure 11, the reboiler heat duty is decreasing significantly by increasing MEA concentration. Reboiler heat duty was decreased 3-10 fold depending on the $CO_2$ loading. That is because there is less solution to be heated to desorb $CO_2$. $CO_2$ loading in MEA is determined by the stochiometric ratio and the operational parameters. If the $CO_2$ absorbed per mole of MEA stays constant, the $CO_2$ loading in the solution decreases with the addition of water. We reported the $CO_2$ loadings we achieved with pure MEA and at varying MEA concentrations in Fig. A.11. $CO_2$ loading was higher when pure MEA was used. As it can be seen from the Figure 11, a higher $CO_2$ loading also leads to a significantly lower reboiler heat duty.

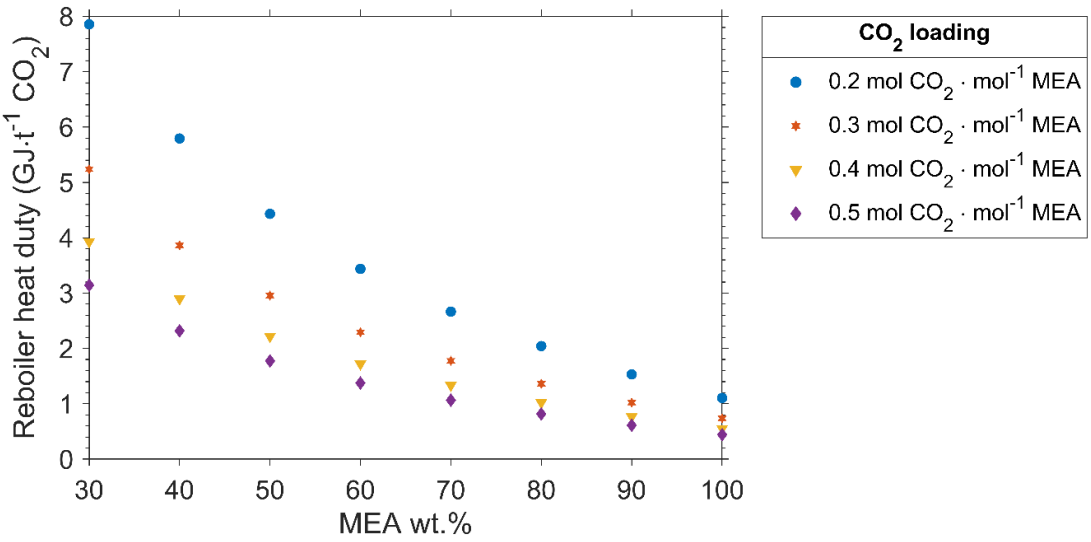


Figure 11. Reboiler heat duty at different MEA concentrations. The $CO_2$ loading refers to the difference between $CO_2$ loadings rich and lean $CO_2$ loadings.

Since the $CO_2$ absorption into different MEA concentrations at the same $CO_2$ loadings resulted in similar levels of carbamate formation up to 70 wt.% of MEA, the heat of absorption (or desorption) is expected to be similar for MEA up to 70 wt.%. After that, an increase in the heat of absorption is expected due to the increased carbamate formation. We have already offered to mix pure MEA with some water but keep the water amount minimal. However, more work is necessary to see the effects of addition of water to pure MEA during desorption. Desorption kinetics from pure MEA is out of the scope of this work. However, the analysis we have done here also applies to using 70 wt.% MEA both in the absorption and desorption column. This work shows that decreasing the water amount in the overall process can result in significant energy savings.

#### 3.2.9.3. Further concerns about using high MEA concentrations

MEA might be explosive if flue gas contains oxygen. The same concern applies for packed columns. The lower and upper explosions limits for MEA in air are 3.0% and 23.5 vol. %, respectively [61]. In this work, the highest aerosol number concentration was obtained as 14336 $cm^{-3}$ in the middle of the spray cone (Fig. A.4). With the highest expected D32 of MEA (110 µm), aerosol volume concentration is calculated as 0.01 $cm^3.cm^{-3}$ (1 vol.%). Since oxygen concentration in the flue gas is also much lower than that of air, this system is expected to work below the explosion limits. However, there might be some differences in the explosion limits when aerosols are used. Therefore, the lower and the upper explosion limits of MEA spray need be tested before it is used with industrial flue gases. We believe that this issue can be tacked relatively easily once the lower and upper explosion limits are known.

One of the main challenges of using high MEA concentrations would be the rate of corrosion, which can be expected to increase as MEA is corrosive. This issue can be tackled to some degree by using resistant materials such as stainless steel. Still, the life of the equipment is expected to be reduced while the frequency of the maintenance might need to be increased. In addition, the formation of heat-stable salts and heat generated during the absorption process might affect the economics. Therefore, more work is necessary to evaluate the effect of using pure MEA on the economics of the process. A detailed techno-economic study will be performed in a follow-up paper with several different process configurations using point sources.

## 4. Conclusions

Conventionally, an aqueous 30 wt.% MEA solution is used due to corrosivity and high viscosity of MEA. Although there is a large body of research on replacing water with organic water-lean solvents, $CO_2$ absorption with pure chemical absorbents such as MEA has not been studied so far. This is because high MEA concentrations are believed to decrease $K_G a$ to prohibitively low values due to the high viscosity of MEA. However, in this study, $K_G a$ was obtained as 11.7 $kmol \cdot m^{-3} \cdot kPa^{-1} \cdot h^{-1}$ with pure MEA, which is significantly higher than the literature values. The increase in $K_G a$ can be associated to more available MEA molecules at gas-liquid interface when pure MEA is used. The effects of several parameters on $K_G a$ and absorption efficiency were studied. The results of the droplet size analysis indicated that interfacial areas increased from 45.3 and 76.0 $m^2.m^{-3}$ for MEA with increasing liquid flow rates. As a result, $K_G a$ increased with increasing liquid flow rates. In addition, $K_G a$ increased with increasing MEA concentration and decreasing $CO_2$ concentration. Gas flow rate did not change $K_G a$ significantly. Absorption efficiencies as high as 99% have been reached. Absorption efficiency is most prominently determined by the ratio of the inlet MEA to $CO_2$ molar concentrations. $^{13}$C-NMR studies revealed that at the same $CO_2$ loadings, similar carbamate levels were obtained up to 70 wt.% MEA. Carbamate formation increased at 90 wt.% MEA and with pure MEA. High $K_G a$ and absorption efficiency at high MEA concentrations will require smaller absorption column for $CO_2$ capture. In addition, a simplified analysis on reboiler heat duty showed that reducing the water amount can lead to 3-10 fold decrease in reboiler heat duty..

## Acknowledgements

This research was funded by VLAIO as a part of Catalisti Moonshot program in Belgium with the project named “Intensification of CO2 Capture Processes” (HBC.2019.0109 - CAPTIN). The authors declare no competing interests.

## Nomenclature

| | |
|---|---|
| $C_{CO2}$ | $CO_2$ molar concentration ($mol \cdot L^{-1}$) |
| $C_p$ | molar heat capacity ($kJ \cdot kg^{-1} \cdot K^{-1}$), |
| $D$ | droplet diameter (m) |

| | |
|---|---|
| $D_{CO2}$ | diffusion coefficient of $CO_2$ ($m^2.s^{-1}$) |
| $E$ | enhancement factor of the reaction |
| $k_G$ | gas side mass transfer coefficient ($kmol \cdot m^{-2} \cdot kPa^{-1} \cdot h^{-1}$) |
| $k_L$ | liquid side mass transfer coefficient ($m \cdot h^{-1}$) |
| $K_G a$ | overall mass transfer coefficient ($kmol \cdot m^{-3} \cdot kPa^{-1} \cdot h^{-1}$) |
| G | gas flow rate ($L \cdot min^{-1}$) |
| $G_{inert}$ | inert gas velocity ($kmol \cdot m^{-2} \cdot h^{-1}$) |
| $H$ | Henry's coefficient ($kPa.m^3.kmol^{-1}$) |
| L | liquid flow rate ($ml \cdot min^{-1}$) |
| $M_{CO2}$ | molecular weight of $CO_2$ ($kg \cdot mol^{-1}$) |
| $M_{soln}$ | molecular weight of the solution ($kg.mol^{-1}$) |
| $t_{99}$ | time it takes for the $CO_2$ concentration to rise from 0 to 99% of the solubility (s) |
| $P$ | total gas pressure (kPa) |
| $p_{H2O}$ | partial pressure of water vapor in the gas phase at the desorber outlet (kPa), |
| $p_{CO2}$ | partial pressure of $CO_2$ in the gas phase at the desorber outlet (kPa), |
| $Q_{desorption}$ | energy required for desorption (or absorption) ($GJ \cdot ton^{-1}\ CO_2$) |
| $Q_{regeneration}$ | regeneration energy ($GJ \cdot ton^{-1}\ CO_2$) |
| $Q_{vaporization}$ | latent heat of vaporization ($GJ \cdot ton^{-1}\ CO_2$) |
| $T_{reb}$ | temperatures in the reboiler (K) |
| $T_{feed}$ | temperatures at the inlet of the desorption column (K) |
| $w_{MEA}$ | MEA weight percentage ($kg\ MEA.kg^{-1}$ solution) |
| $X_{MEA}$ | molar fraction of MEA in the solution |
| $Y_{CO2}$ | mole ratio of $CO_2$ in the gas phase |

$y_{CO2}$ mole fraction of $CO_2$ in the gas phase

$y_{CO2}^*$ mole fraction of $CO_2$ in equilibrium with the liquid phase

$Z$ height of the reactor (m)

**Greek letters**

$\alpha$ interfacial area for mass transfer ($m^2.m^{-3}$)

γ surface tension ($N.m^{-1}$)

$\Delta\alpha$ the difference in rich and lean $CO_2$ loading (mol $CO_2 \cdot$ $mol^{-1}$ MEA)

$\Delta H_{vap,H2O}$ molar latent heat of water ($kJ{\cdot}mol^{-1}$)

$\Delta H_{des,CO2}$ heat of desorption or absorption ($kJ{\cdot}mol^{-1}$).

μ viscosity of the liquid (Pa.s)

ρ density of the liquid ($kg.m^{-3}$)

**Subscripts**

in inlet of the reactor

out outlet of the reactor

## References


[1] M. Wang, A. Lawal, P. Stephenson, J. Sidders, C. Ramshaw, Post-combustion CO2 capture with chemical absorption: A state-of-the-art review, Chemical Engineering Research and Design. 89 (2011) 1609–1624. https://doi.org/10.1016/j.cherd.2010.11.005.

[2] M. Afkhamipour, M. Mofarahi, Review on the mass transfer performance of CO2 absorption by amine-based solvents in low- and high-pressure absorption packed columns, RSC Advances. 7 (2017) 17857–17872. https://doi.org/10.1039/c7ra01352c.

[3] I. Sreedhar, T. Nahar, A. Venugopal, B. Srinivas, Carbon capture by absorption – Path covered and ahead, Renewable and Sustainable Energy Reviews. 76 (2017) 1080–1107.

[4] M.R.M. Abu-Zahra, L.H.J. Schneiders, J.P.M. Niederer, P.H.M. Feron, G.F. Versteeg, CO2 capture from power plants. Part I. A parametric study of the technical performance based on monoethanolamine, International Journal of Greenhouse Gas Control. 1 (2007) 37–46. https://doi.org/10.1016/S1750-5836(06)00007-7.

[5] J.N. Knudsen, J.N. Jensen, P.J. Vilhelmsen, O. Biede, Experience with CO2 capture from coal flue gas in pilot-scale: Testing of different amine solvents, in: Energy Procedia, 2009: pp. 783–790. https://doi.org/10.1016/j.egypro.2009.01.104.

[6] S. Zimmermann, M.O. Schmid, B. Klein, G. Scheffknecht, Experimental studies on spray absorption with the post combustion CO2 capture pilot-plant CASPAR, Energy Procedia. 114 (2017) 1325–1333. https://doi.org/10.1016/j.egypro.2017.03.1252.

[7] M. Koller, D. Wappel, N. Trofaier, G. Gronald, Test results of CO2 spray scrubbing with monoethanolamine, in: Energy Procedia, Elsevier Ltd, 2011: pp. 1777–1782. https://doi.org/10.1016/j.egypro.2011.02.053.

[8] O. Seyboth, S. Zimmermann, B. Heidel, G. Scheffknecht, Development of a spray scrubbing process for post combustion CO2 capture with amine based solvents, Energy Procedia. 63 (2014) 1667–1677. https://doi.org/10.1016/j.egypro.2014.11.176.

[9] J. Kuntz, A. Aroonwilas, Performance of spray column for CO2 capture application, Industrial & Engineering Chemistry Research. 47 (2008) 145–153. https://doi.org/10.1021/ie061702l.

[10] X.M. Wu, Z. Qin, Y.S. Yu, Z.X. Zhang, Experimental and numerical study on CO2 absorption mass transfer enhancement for a diameter-varying spray tower, Applied Energy. 225 (2018) 367–379. https://doi.org/10.1016/j.apenergy.2018.04.053.

[11] A. Dey, A. Aroonwilas, CO2 absorption into MEA-AMP blend: Mass transfer and absorber height index, in: Energy Procedia, 2009: pp. 211–215. https://doi.org/10.1016/j.egypro.2009.01.030.

[12] M. Afkhamipour, M. Mofarahi, Comparison of rate-based and equilibrium-stage models of a packed column for post-combustion CO2 capture using 2-amino-2-methyl-1-propanol (AMP) solution, International Journal of Greenhouse Gas Control. 15 (2013) 186–199. https://doi.org/10.1016/j.ijggc.2013.02.022.

[13] A. Aroonwilas, P. Tontiwachwuthikul, High-efficiency structured packing for CO2 separation using 2-amino-2-methyl-1-propanol (AMP), Separation and Purification Technology. 12 (1997) 67–79.

[14] D. deMontigny, P. Tontiwachwuthikul, A. Chakma, Parametric studies of carbon dioxide absorption into highly concentrated monoethanolamine solutions, The Canadian Journal of Chemical Engineering. 79 (2001) 137–142.

[15] A. Aroonwilas, P. Tontiwachwuthikul, Mass transfer coefficients and correlation for CO2 absorption into 2-Amino-2-methyl-1-propanol (AMP) using structured packing, Industrial and Engineering Chemistry Research. 37 (1998) 569–575. https://pubs.acs.org/sharingguidelines.

[16] W. Li, X. Zhao, B. Liu, Z. Tang, Mass transfer coefficients for CO2 absorption into aqueous ammonia using structured packing, Industrial and Engineering Chemistry Research. 53 (2014) 6185–6196. https://doi.org/10.1021/ie403097h.

[17] B. Xu, H. Gao, X. Luo, H. Liao, Z. Liang, Mass transfer performance of CO2 absorption into aqueous DEEA in packed columns, International Journal of Greenhouse Gas Control. 51 (2016) 11–17. https://doi.org/10.1016/j.ijggc.2016.05.004.

[18] B. Zhao, Y. Su, G. Cui, Post-combustion CO2 capture with ammonia by vortex flow-based multistage spraying: Process intensification and performance characteristics, Energy. 102 (2016) 106–117. https://doi.org/10.1016/j.energy.2016.02.056.

[19] K.H. Javed, T. Mahmud, E. Purba, The CO2 capture performance of a high-intensity vortex spray scrubber, Chemical Engineering Journal. 162 (2010) 448–456. https://doi.org/10.1016/j.cej.2010.03.038.

[20] R.R. Wanderley, D.D.D. Pinto, H.K. Knuutila, From hybrid solvents to water-lean solvents – A critical and historical review, Separation and Purification Technology. 260 (2021) 118193. https://doi.org/10.1016/j.seppur.2020.118193.

[21] D.J. Heldebrant, P.K. Koech, V.A. Glezakou, R. Rousseau, D. Malhotra, D.C. Cantu, Water-lean solvents for post-combustion CO2 capture: fundamentals, uncertainties, opportunities, and

outlook, Chemical Reviews. 117 (2017) 9594–9624. https://doi.org/10.1021/acs.chemrev.6b00768.

[22] M. Ramdin, T.W. de Loos, T.J.H. Vlugt, State-of-the-art of CO2 capture with ionic liquids, Industrial and Engineering Chemistry Research. 51 (2012) 8149–8177. https://doi.org/10.1021/ie3003705.

[23] O.R. Rivas, J.M. Prausnitz, Sweetening of sour natural gases by mixed-solvent absorption: solubilities of ethane, carbon dioxide, and hydrogen sulfide in mixtures of physical and chemical solvents, AICHE Journal . 25 (1979) 975–983.

[24] B.E. Roberts, A.E. Mather, Solubility of CO2 and H2S in a mixed solvent, Chemical Engineering Communications. 72 (1988) 201–211. https://doi.org/10.1080/00986448808940017.

[25] R.R. Wanderley, D.D.D. Pinto, H.K. Knuutila, Investigating opportunities for water-lean solvents in CO2 capture: VLE and heat of absorption in water-lean solvents containing MEA, Separation and Purification Technology. 231 (2020) 115883. https://doi.org/10.1016/j.seppur.2019.115883.

[26] Y. Yuan, G.T. Rochelle, CO2 absorption rate in semi-aqueous monoethanolamine, Chemical Engineering Science. 182 (2018) 56–66. https://doi.org/10.1016/j.ces.2018.02.026.

[27] R.R. Wanderley, H.K. Knuutila, Mapping diluents for water-lean solvents: A parametric study, Industrial and Engineering Chemistry Research. 59 (2020) 11656–11680. https://doi.org/10.1021/acs.iecr.0c00940.

[28] R.R. Wanderley, Y. Yuan, G.T. Rochelle, H.K. Knuutila, CO2 solubility and mass transfer in water-lean solvents, Chemical Engineering Science. 202 (2019) 403–416. https://doi.org/10.1016/j.ces.2019.03.052.

[29] F. de Meyer, C. Bignaud, The use of catalysis for faster CO2 absorption and energy-efficient solvent regeneration: An industry-focused critical review, Chemical Engineering Journal. 428 (2022) 131264. https://doi.org/10.1016/j.cej.2021.131264.

[30] R.H. Weiland, J.C. Dingman, D.B. Cronin, Heat capacity of aqueous monoethanolamine, diethanolamine, N-methyldiethanolamine, and N-methyldiethanolamine-based blends with

carbon dioxide, Journal of Chemical Engineering Data. 42 (1997) 1004–1006. https://pubs.acs.org/sharingguidelines.

[31] W.C. Hinds, Aerosol technology: properties, behavior, and measurements of airborne particles, 2nd ed., John Wiley & Sons, Inc, 1999.

[32] Fiji, (n.d.). https://imagej.net/imaging/ (accessed January 24, 2022).

[33] MATLAB 2020b, (n.d.). https://nl.mathworks.com/help/matlab/index.html (accessed January 24, 2022).

[34] Hielscher Ultrasound Technology, Operation manual of Hielscher UP200St , n.d. https://www.hielscher.com/up200st-powerful-ultrasonic-lab-homogenizer.htm (accessed October 28, 2021).

[35] B. Lv, B. Guo, Z. Zhou, G. Jing, Mechanisms of CO2 capture into monoethanolamine solution with different CO2 loading during the absorption / desorption processes, Environmental Science and Technology. 49 (2015) 10728–10735. https://doi.org/10.1021/acs.est.5b02356.

[36] W. Böttinger, M. Maiwald, H. Hasse, Online NMR spectroscopic study of species distribution in MEA-H2O-CO2 and DEA-H2O-CO2, Fluid Phase Equilibria. 263 (2008) 131–143. https://doi.org/10.1016/j.fluid.2007.09.017.

[37] K.H. Javed, T. Mahmud, E. Purba, Enhancement of mass transfer in a spray tower using swirling gas flow, Chemical Engineering Research and Design. 84 (2006) 465–477. https://doi.org/10.1205/cherd.05119.

[38] Y. Tamhankar, B. King, J. Whiteley, T. Cai, K. McCarley, M. Resetaris, C. Aichele, Spray absorption of CO2 into monoethanolamine: Mass transfer coefficients, dropsize, and planar surface area, Chemical Engineering Research and Design. 104 (2015) 376–389. https://doi.org/10.1016/j.cherd.2015.08.012.

[39] A. Bandyopadhyay, M.N. Biswas, CO2 capture in a spray column using a critical flow atomizer, Separation and Purification Technology. 94 (2012) 104–114. https://doi.org/10.1016/j.seppur.2011.11.039.

[40] K.A. Ramisetty, A.B. Pandit, P.R. Gogate, Investigations into ultrasound induced atomization, Ultrasonics Sonochemistry. 20 (2013) 254–264. https://doi.org/10.1016/j.ultsonch.2012.05.001.

[41] E. Kayahan, D. Urbani, P. Dambruoso, A. Massi, L. Braeken, T. van Gerven, M. Enis Leblebici, Overcoming mass and photon transfer limitations in a scalable reactor: Oxidation in an aerosol photoreactor, Chemical Engineering Journal. 408 (2021) 127357. https://doi.org/10.1016/j.cej.2020.127357.

[42] P. v. Danckwerts, The reaction of CO2 with ethanolamines, Chemical Engineering Science. 34 (1979) 443–446. https://doi.org/10.1016/0009-2509(79)85087-3.

[43] M. Caplow, Kinetics of Carbamate Formation and Breakdown, J Am Chem Soc. 90 (1967) 6795–6803.

[44] D.C. Montgomery, G.C. Runger, Applied Statistics and Probability for Engineers, 5th ed., John Wiley and Sons, Inc. , 2011.

[45] P.D. Vaidya, E.Y. Kenig, CO2-alkanolamine reaction kinetics: A review of recent studies, Chemical Engineering and Technology. 30 (2007) 1467–1474. https://doi.org/10.1002/ceat.200700268.

[46] J.E. Crooks, J.P. Donnellan, Kinetics and mechanism of the reaction between carbon dioxide and amines in aqueous solution, Journal of the Chemical Society, Perkin Transactions II. (1989) 331–333.

[47] E.F. da Silva, H.F. Svendsen, Ab initio study of the reaction of carbamate formation from CO2 and alkanolamines, Industrial and Engineering Chemistry Research. 43 (2004) 3413–3418. https://doi.org/10.1021/ie030619k.

[48] T.L. Donaldson, Y.N. Nguyen, Carbon dioxide reaction kinetics and transport in aqueous amine membranes, Industrial and Engineering Chemistry Fundamentals. 19 (1980) 260–266.

[49] H. bin Xie, Y. Zhou, Y. Zhang, J.K. Johnson, Reaction mechanism of monoethanolamine with CO2 in aqueous solution from molecular modeling, Journal of Physical Chemistry A. 114 (2010) 11844–11852. https://doi.org/10.1021/jp107516k.

[50] G.Q. Wang, X.G. Yuan, K.T. Yu, Review of mass-transfer correlations for packed columns, Industrial and Engineering Chemistry Research. 44 (2005) 8715–8729. https://doi.org/10.1021/ie050017w.

[51] P. v. Kortunov, M. Siskin, L.S. Baugh, D.C. Calabro, In situ nuclear magnetic resonance mechanistic studies of carbon dioxide reactions with liquid amines in non-aqueous systems: Evidence for the formation of carbamic acids and zwitterionic species, Energy and Fuels. 29 (2015) 5940–5966. https://doi.org/10.1021/acs.energyfuels.5b00985.

[52] A. Aroonwilas, A. Veawab, Characterization and comparison of the CO2 absorption performance into single and blended alkanolamines in a packed column, Industrial and Engineering Chemistry Research. 43 (2004) 2228–2237. https://doi.org/10.1021/ie0306067.

[53] A. Aroonwilas, A. Veawab, P. Tontiwachwuthikul, Behavior of the mass-transfer coefficient of structured packings in CO2 absorbers with chemical reactions, Industrial and Engineering Chemistry Research. 38 (1999) 2044–2050. https://doi.org/10.1021/ie980728c.

[54] X. Wu, Y. Yu, Z. Qin, Z. Zhang, Performance of CO2 absorption in a diameter-varying spray tower, Chinese Journal of Chemical Engineering. 25 (2017) 1109–1114. https://doi.org/10.1016/j.cjche.2017.03.013.

[55] F. Bougie, X. Fan, Microwave regeneration of monoethanolamine aqueous solutions used for CO2 capture, International Journal of Greenhouse Gas Control. 79 (2018) 165–172. https://doi.org/10.1016/j.ijggc.2018.10.008.

[56] J. Oexmann, A. Kather, Minimising the regeneration heat duty of post-combustion CO2 capture by wet chemical absorption: The misguided focus on low heat of absorption solvents, International Journal of Greenhouse Gas Control. 4 (2010) 36–43. https://doi.org/10.1016/j.ijggc.2009.09.010.

[57] I. Kim, K.A. Hoff, T. Mejdell, Heat of absorption of CO2 with aqueous solutions of MEA: New experimental data, in: Energy Procedia, Elsevier Ltd, 2014: pp. 1446–1455. https://doi.org/10.1016/j.egypro.2014.11.154.

[58] I. Kim, H.F. Svendsen, Heat of absorption of carbon dioxide (CO2) in monoethanolamine (MEA) and 2-(aminoethyl)ethanolamine (AEEA) solutions, Industrial and Engineering Chemistry Research. 46 (2007) 5803–5809. https://doi.org/10.1021/ie0616489.

[59] R.H. Perry, D.W. Green, J.O. Maloney, eds., Perry's Chemical Engineers' Handbook, 7th editio, McGraw-Hill, 1997.

[60] Y. Chen, T. Shih, M. Li, Heat capacity of aqueous mixtures of monoethanolamine with n-methyldiethanolamine, Journal of Chemical Engineering Data. 46 (2001) 51–55. https://doi.org/10.1021/je0000367.

[61] U.S. Department of Health & Human Services, The National Institute for Occupational Safety and Health (NIOSH), (n.d.). https://www.cdc.gov/niosh/npg/npgd0256.HTML (accessed January 25, 2022).

# Appendix

# A new look to the old solvent: Mass transfer performance and mechanism of $CO_2$ absorption into pure monoethanolamine in a spray column

Emine Kayahan[1], Ulderico Di Caprio[1], Annelot Van den Bogaert[1], Mohammed N. Khan[2], Metin Bulut[2], Leen Braeken[1], Tom Van Gerven[3], M. Enis Leblebici[1,*]

[1] *Center for Industrial Process Technology, Department of Chemical Engineering, KU Leuven, Agoralaan Building B, 3590 Diepenbeek, Belgium*

[2] *Business Unit Separation and Conversion Technology, Flemish Institute for Technological Research (VITO), Boeretang 200, 2400 Mol, Belgium*

[3] *Process Engineering for Sustainable Systems, Department of Chemical Engineering, KU Leuven, Celestijnenlaan 200F, B-3001 Heverlee, Belgium*

*Corresponding author (muminenis.leblebici@kuleuven.be)

## Nomenclature

Am tip amplitude (m)

C velocity of sound in liquid medium (m/s)

D32 Sauter mean droplet diameter

I intensity of ultrasound ($W.m^{-2}$)

Q volumetric liquid flow rate ($m^3.s^{-1}$)

*Dimensionless numbers*

Oh modified Ohnesorge number $= \frac{\mu}{f\ Am\ \rho}$

We modified Weber number $= \frac{f\ Q\ \rho}{\gamma}$

In intensity number $= \frac{f^2 Am^4}{C\ Q}$

*Greek letters*

μ viscosity of the liquid (Pa.s)

ρ density of the liquid ($kg.m^{-3}$)

γ surface tension ($N.m^{-1}$)

## A.1. Physical properties of monoethanolamine (MEA) and propylene glycol (PG) solutions

The viscosities of MEA solutions as a function of the weight concentration are given in Fig. A.1a. Our experimental measurements are in line with the values reported at 20°C by Arachchige et al. [1]. The viscosity of propylene glycol (PG) solutions as a function of weight fraction are given in Fig. A.1b. The values are compared with the work of George and Sastry [2].

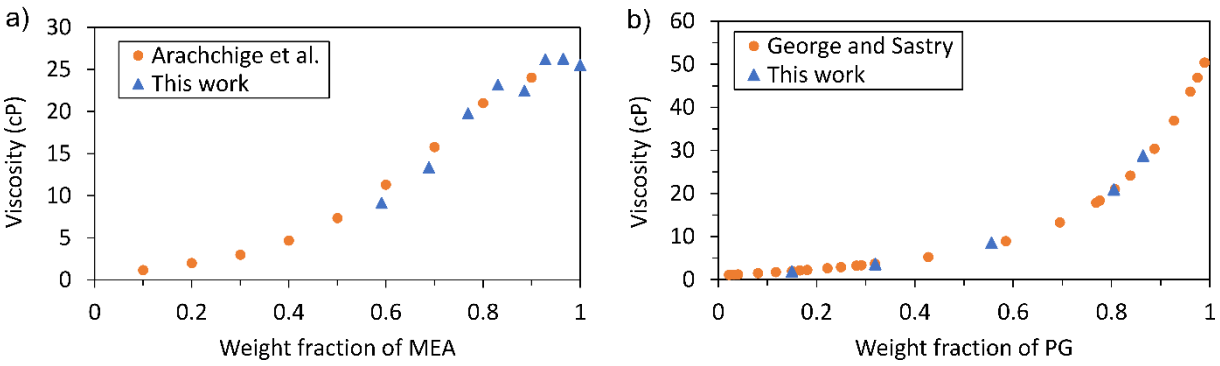


Fig. A.1. Comparison of the viscosity of a) MEA solutions in terms of weight fraction with the literature data [1], b) PG solutions in terms of weight fraction with the literature data [2].

Surface tension of MEA solutions at different weight fractions at 20°C are shown in Fig. A.2a. The results are compared with literature data at 30°C [3]. The data is slightly different than literature data due to the difference in temperature. The surface tension of PG solutions at 20°C at various weight percentages are shown in Fig. A.2b. The results were in line with the literature data at 20°C [4].

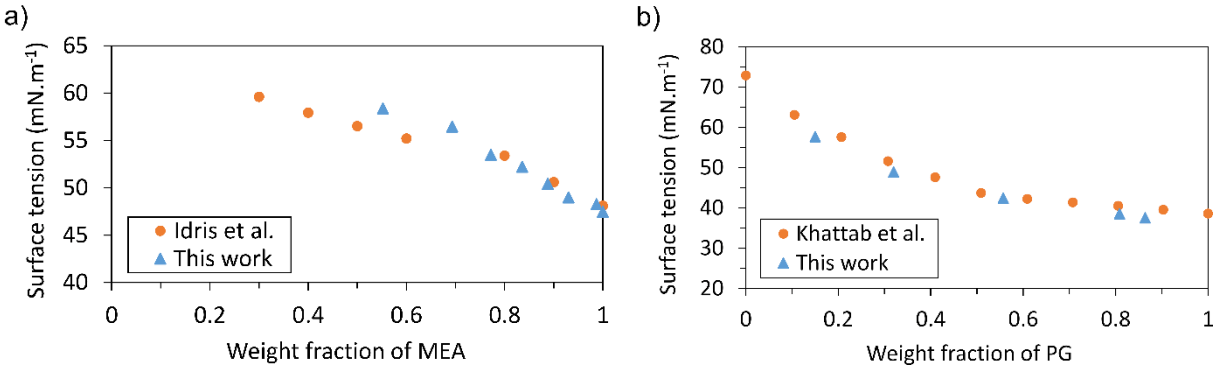


Fig. A.2. Comparison of the surface tension of a) MEA solutions in terms of weight fraction with the literature data [3], b) PG solutions in terms of weight fraction with the literature data [4].

## A.2. Calculation of Sauter mean droplet diameter of an ultrasonic nozzle from an empirical equation

The droplet sizes of the PG solution predicted by the empirical equation (Equation (12)) which was offered by Ramisetty et al. [5]. Names of the symbols are given in the Nomenclature. Comparison between experimental and predicted D32 values are shown in Fig. A.3.

$$D32 = 0.00154\left(\frac{\pi\gamma}{\rho f^2}\right)^{0.33}\left(1+\left(\frac{\pi\gamma}{\rho f^2}\right)^{-0.2} Oh^{-0.111} We^{0.154} In^{-0.333}\right) \quad (12)$$

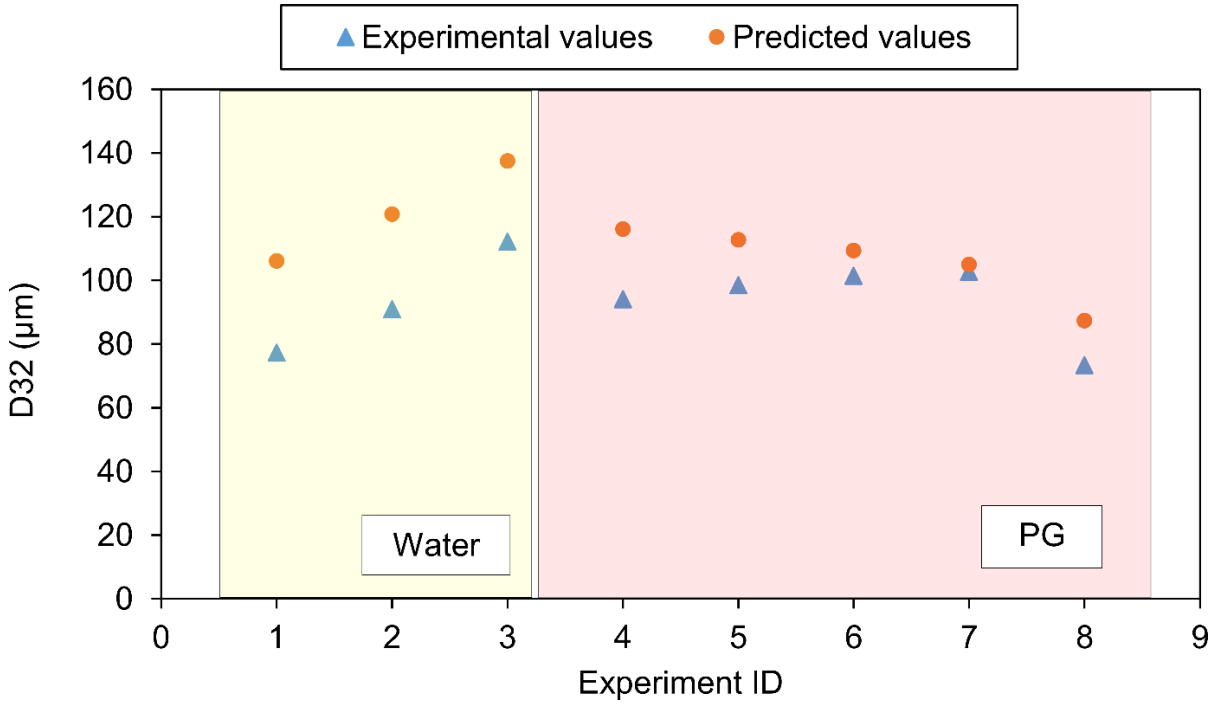


Fig. A.3. Comparison of experimental and predicted values of Sauter mean droplet diameter of water at various flow rates and PG at various weight percentages. The predicted values are calculated by using the empirical equation provided by Ramisetty et al. [5].

## A.3. Results of droplet size analysis

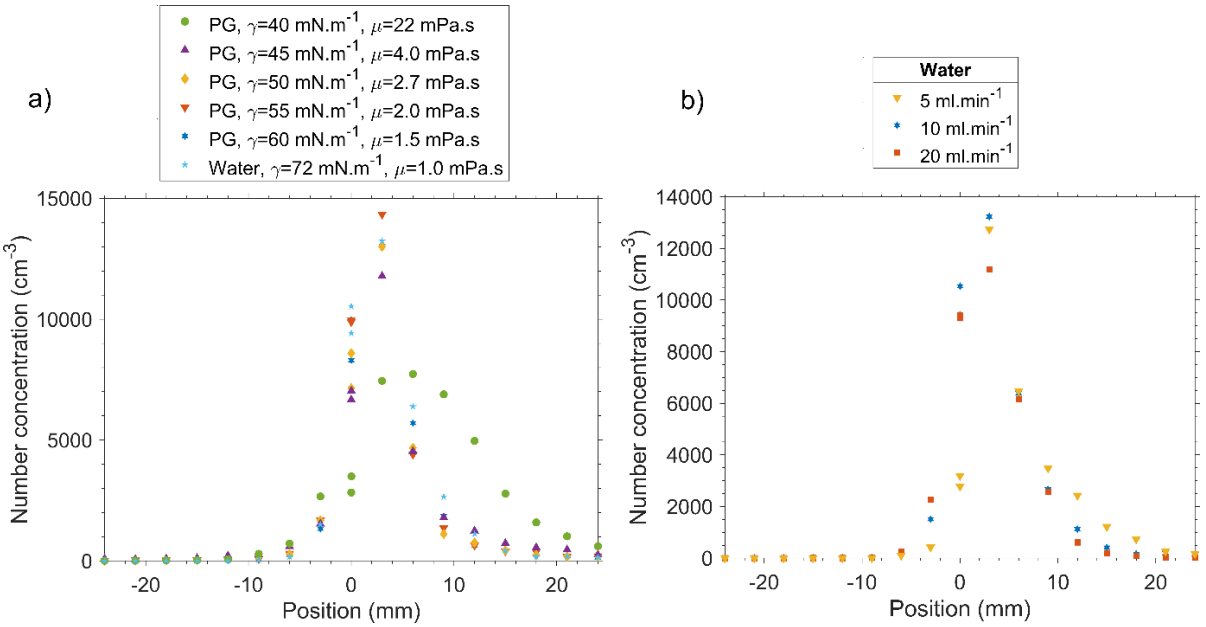


Fig. A.4. Number concentration in position. Zero position is the center of the nozzle tip. a) Number concentration of water and PG at various viscosities and surface tensions, b) Number concentration of water at several flow rates.

## A.4. Effect of stoichiometric ratio

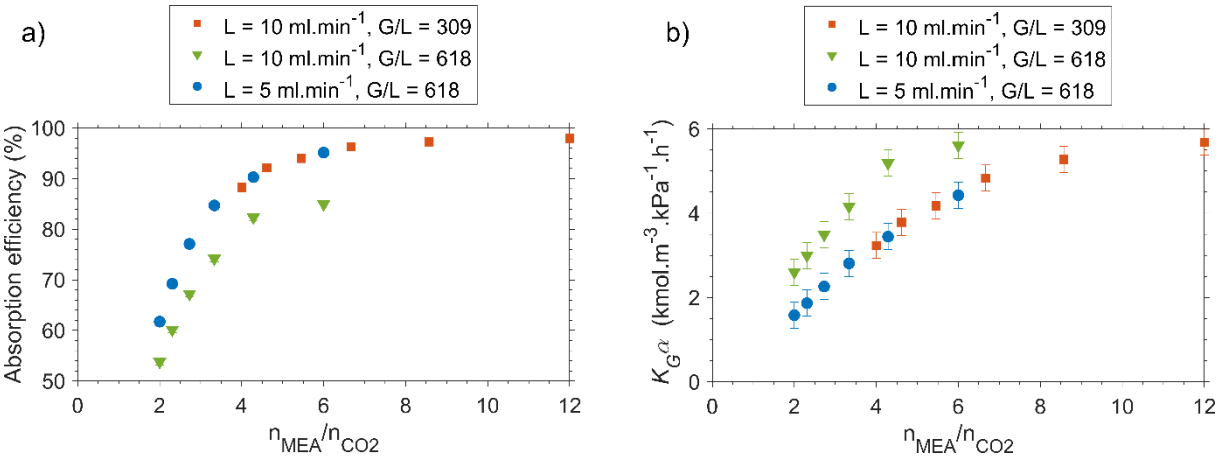


Fig. A.5. Effect of stoichiometric ratio on a) absorption efficiency, b) $K_G a$. The stoichiometric ratio was changed by changing $CO_2$ concentration.

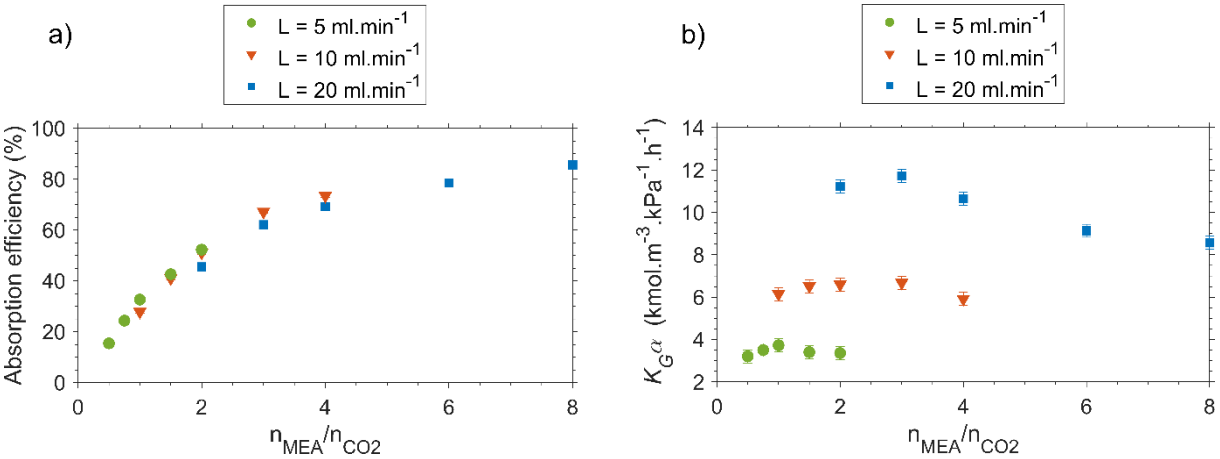


Fig. A.6. Effect of stoichiometric ratio on a) absorption efficiency, b) $K_G a$. The stoichiometric ratio was changed by changing gas flow rate.

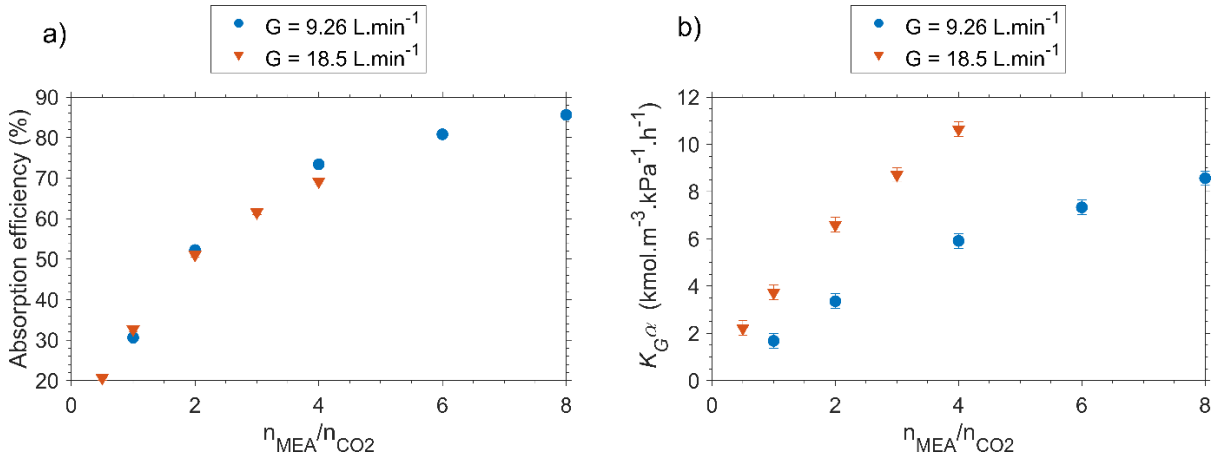


Fig. A.7. Effect of stoichiometric ratio on a) absorption efficiency, b) $K_G a$. The stoichiometric ratio was changed by changing liquid flow rate.

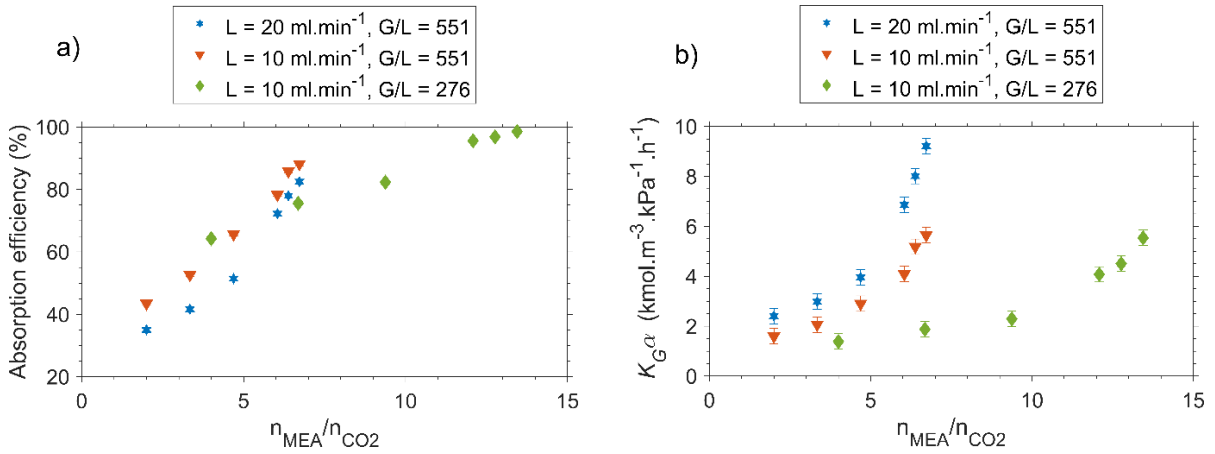


Fig. A.8. Effect of stoichiometric ratio on a) absorption efficiency, b) $K_G a$. The stoichiometric ratio was changed by changing MEA concentration.

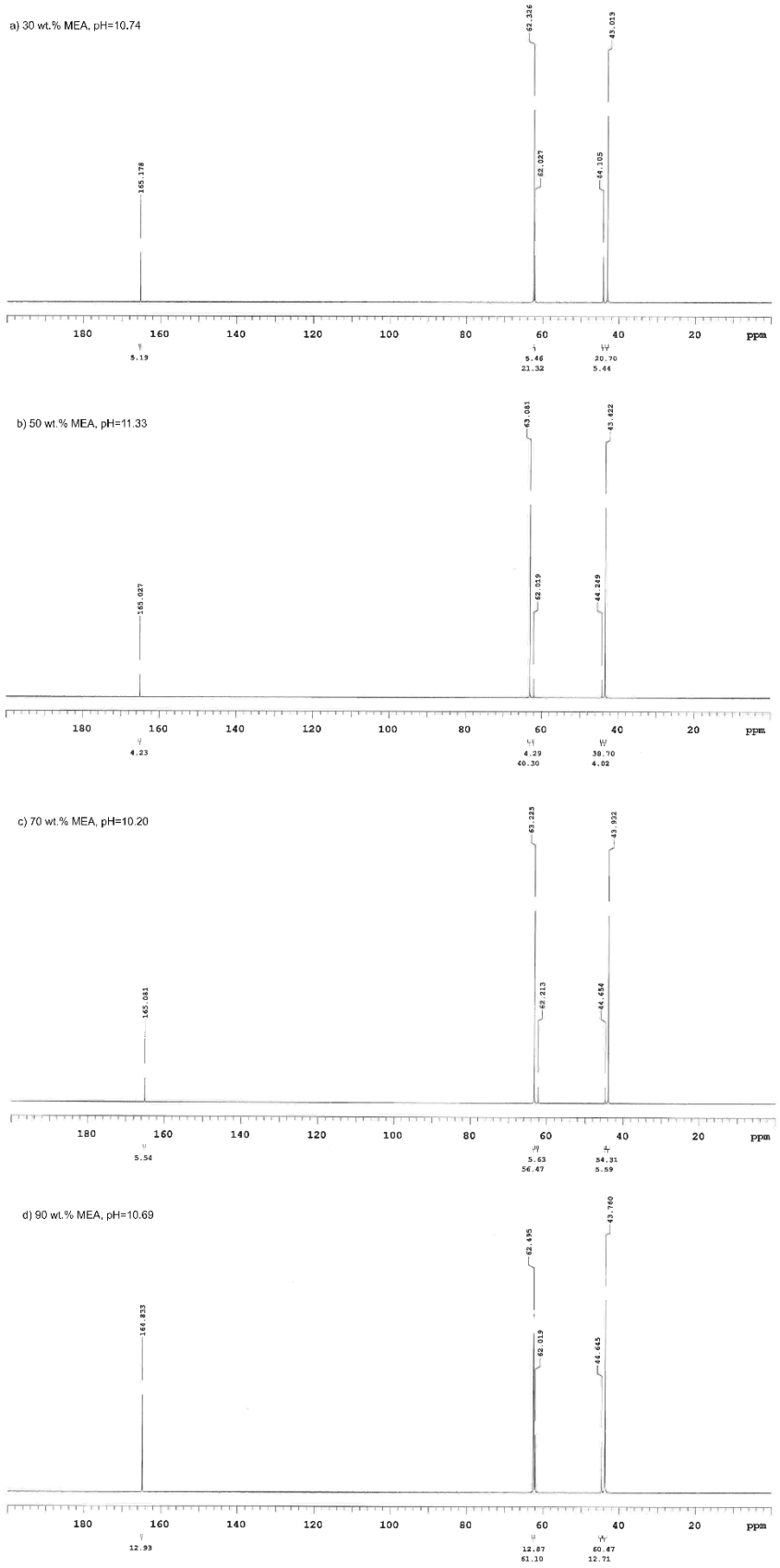


Fig. A.9. $^{13}$C-NMR spectra of $CO_2$-loaded MEA at various concentrations a) 30 wt.% MEA, b) 50 wt.% MEA, c) 70 wt.% MEA, d) 90 wt.% MEA.

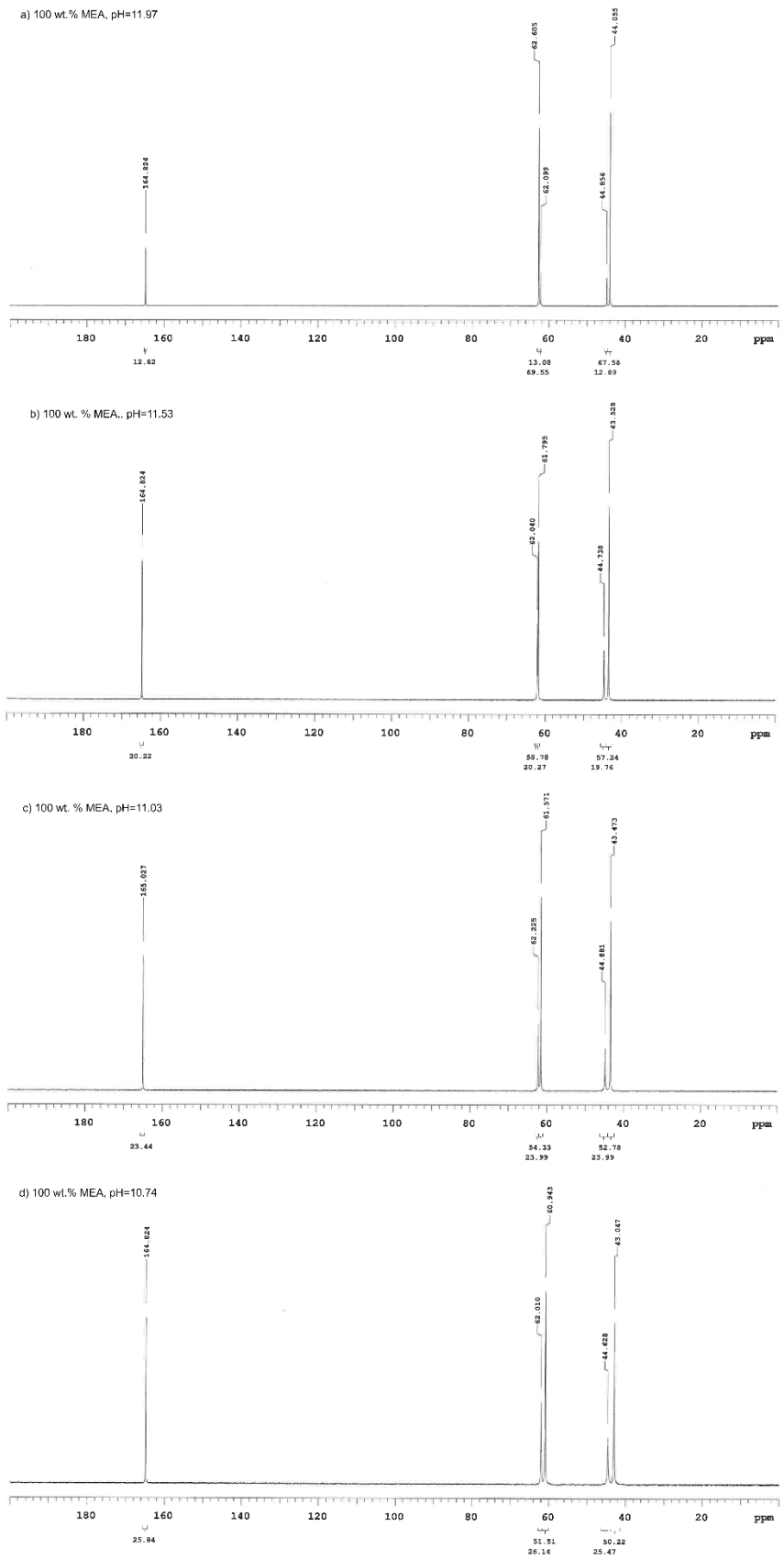


Fig. A.10. $^{13}$C-NMR spectra of $CO_2$-loaded pure MEA at various $CO_2$ concentrations a) pH=11.97, b) pH=11.53, c) pH=11.03, d) pH=10.74.

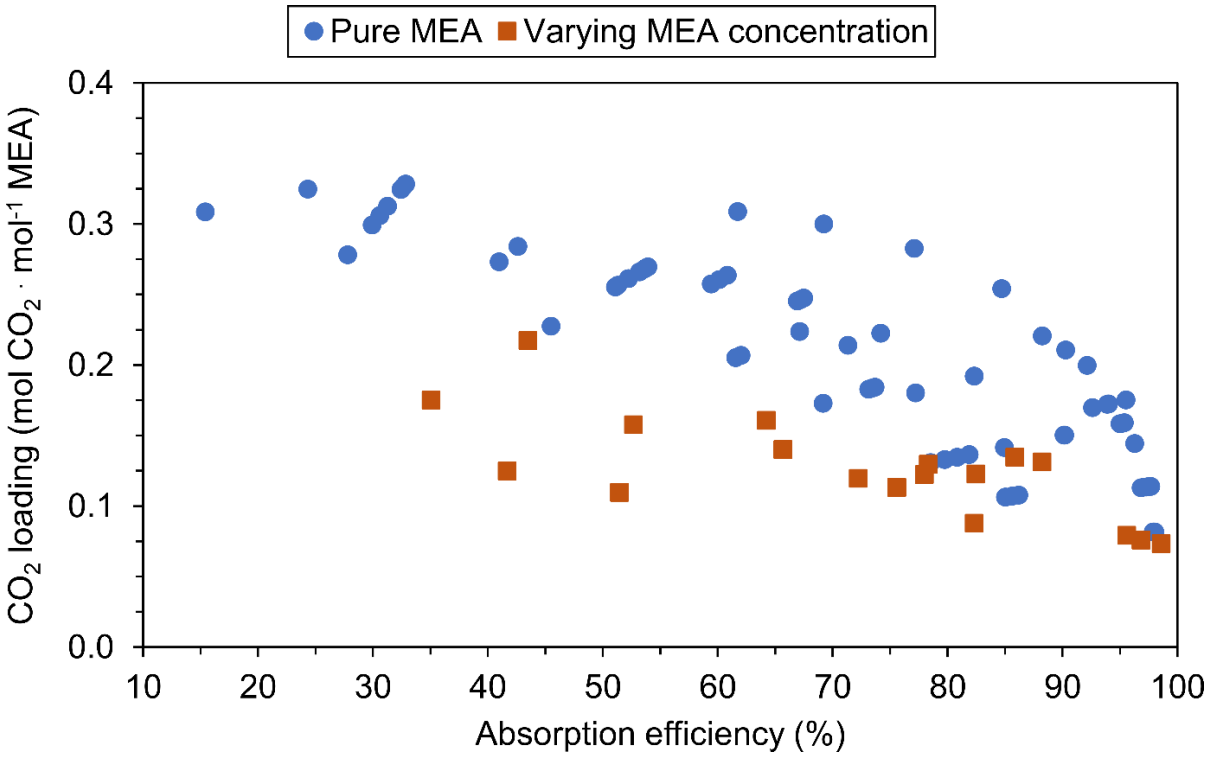


Fig. A.11. $CO_2$ loadings at various absorption efficiencies for pure MEA and varying MEA concentrations.

## References


[1] U.S.P.R. Arachchige, N. Aryal, D.A. Eimer, M.C. Melaaen, Viscosities of pure and aqueous solutions of monoethanolamine (MEA), diethanolamine (DEA) and N-methyldiethanolamine (MDEA), Annual Transactions of the Nordic Rheology Society . 21 (2013) 299–306.

[2] J. George, N. v. Sastry, Densities, dynamic viscosities, speeds of sound, and relative permittivities for water + alkanediols (propane-1,2- and -1,3-diol and butane-1,2-, -1,3-, -1,4-, and -2,3-diol) at different temperatures, Journal of Chemical and Engineering Data. 48 (2003) 1529–1539. https://doi.org/10.1021/je0340755.

[3] Z. Idris, J. Han, S. Jayarathna, D.A. Eimer, Surface tension of alkanolamine solutions: An experimentally based review, in: Energy Procedia, Elsevier Ltd, 2017: pp. 1828–1833. https://doi.org/10.1016/j.egypro.2017.03.1310.

[4] I.S. Khattab, F. Bandarkar, M. Khoubnasabjafari, A. Jouyban, Density, viscosity, surface tension, and molar volume of propylene glycol + water mixtures from 293 to 323 K and correlations by the Jouyban–Acree model, Arabian Journal of Chemistry. 10 (2017) S71–S75. https://doi.org/10.1016/j.arabjc.2012.07.012.

[5] K.A. Ramisetty, A.B. Pandit, P.R. Gogate, Investigations into ultrasound induced atomization, Ultrasonics Sonochemistry. 20 (2013) 254–264. https://doi.org/10.1016/j.ultsonch.2012.05.001.